International Committee for Future Accelerators

Sponsored by the Particles and Fields Commission of IUPAP

Beam Dynamics Newsletter

No. 34

Issue Editor:
D. Rice

Editor in Chief:
W. Chou

August 2004

CONTENTS

1 Foreword

1.1 From the Chairman

Weiren Chou, Fermilab
mail to: chou@fnal.gov

1.1.1 Technology Recommendation for the International Linear Collider

On August 20, 2004 at 12:45 pm (Beijing time), Jonathan Dorfan, Chairman of ICFA and Director of SLAC, made an important announcement to the audience of ICHEP'04, which was taking place at the Beijing International Convention Center. ICFA unanimously approved the recommendation of the International Technology Recommendation Panel (ITRP) to choose the superconducting RF technology, nicknamed "cold" technology, for the International Linear Collider (ILC). This is a major milestone on the long road to reach a TeV-scale electron-positron linear collider. The ILC will be the next major construction project endorsed by the global particle physics community after the CERN LHC. The executive summary of the ITRP report can be found in Section 1.3.

1.1.2 World Accelerator Catalog

As announced in our last Newsletter (No. 33, April 2004), the ICFA Beam Dynamics Panel is in the process of producing a new *World Accelerator Catalog*. This catalog will be a revised and greatly expanded version of the one compiled at the 1992 HEACC. In addition to the printed format, an on-line version with search and update capabilities will be available. The catalog editorial board has been formed and consists of five ICFA Panel members: C. Biscari (LNF-INFN), I. Hofmann (GSI), K-J. Kim (ANL), Y. Mori (KEK) and W. Chou (Fermilab). J-F. Ostiguy (Fermilab) is Technical Advisor. The board held its first meeting on July 19-20, 2004 at Fermilab. The structure of the catalog was decided. Various tables for machine parameter input are being designed. A contractor has been hired to work on the relational database and web site. A letter has been sent out to the director of each institute around the world requesting the appointment of an official contact person(s) for each accelerator. The editors will contact them to collect machine parameters. We will also ask the contact persons to review the parameters before their release and to update them periodically. The scheduled completion date is January 2005. Information about the status of the World Accelerator Catalog Project can be found on the web at http://www bd.fnal.gov/icfabd/

1.1.3 ICFA Workshops and Mini-Workshops

The 32nd ICFA Advanced Beam Dynamics Workshop (ABDW), *ERL2004*, originally scheduled for October 2004, has been postponed to early 2005. The dates are yet to be determined. Please contact the workshop organizers for more information. The

33rd ICFA ABDW, *HB2004*, will take place October 18-22, 2004 at Bensheim, Germany.

The Future Light Sources Working Group sponsored two ICFA mini-workshops, *Physics of Seeded FELs* (June 17-19, 2004, MIT) and *XFEL Short Bunch Measurement and Timing* (July 26-30, 2004, SLAC). Summary reports can be found in Section 3.

1.2 From the Editor

David Rice, LEPP, Cornell University
mail to: dhr1@cornell.edu

The recent decision and widespread endorsement of the Linear Collider ITRP is a vitally important milestone in accelerator development, not only in paving the way for the next stages of R&D work, but also as an indicator of the level of interlaboratory and international cooperation. Included in this newsletter are comments from ICFA BDP Chair Weiren Chou (above), ILCSC Chair Maury Tigner, the Executive summary of the ITRP, and links to more detailed information.

This issue of the ICFA Beam Dynamics Newsletter also has a special section on beam-beam interactions. Throughout the history of colliding beam machines the beam-beam interaction has been one of the most critical phenomena in determining machine performance, yet at the same time one of the least understood.

Advances in computing power and program algorithms have played a large role in our increased understanding of the results of the beam-beam interaction. The simulations are supported by improvements in analytical treatment, both by providing a physical explanation for tracking and measurement results, and by making the tracking algorithms faster and more realistic.

Several machines now operate with significant parasitic crossings - from two to 89. These parasitic crossings can easily limit performance, as has been found in CESR and the Tevetron (see paper by T. Sen). Some machines operate with strong sextupoles and wigglers, adding more lattice nonlinearities to be considered. Including these effects in tracking codes pushes again the need for faster and/or parallel machines (see paper by J. Qiang).

I would like to thank the authors for their excellent work in research and preparation of the papers included in this newsletter.

Following the beam-beam papers are reports from the Workshop on the Physics of Seeded FEL's, the Workshop on XFEL Short Bunch Measurements and Timing, and a status report from the Working Group on Remote Experiments in Accelerator Physics.

1.3 The ITRP Recommendation

1.3.1 Comments from ILCSC Chair

Maury Tigner, LEPP, Cornell University
mail to: mt52@cornell.edu

Late in 2003 the International Linear Collider Steering Committee (ILCSC), acting for ICFA, appointed an International Technology Recommendation Panel to recommend a single technology with which to go forward. The Panel was chaired by Barry Barish, a technically knowledgeable particle physicist and currently Director of the LIGO project. The Panel consisted of 12 members, 4 from each region, Asia, Europe and N. America.

In the course of their work, which has now been completed, they had 6 meeting in April and May and two deliberation meetings, one at Cal Tech, Barish's home institution, in June and in Korea in August. Barish delivered their recommendation to a combined meeting of ILCSC and ICFA during the ICHEP2004 meeting in Bejing on August 19. The recommendation of the superconducting technology was unanimously accepted by ICFA and the ILCSC.

Their work was extremely thorough, each member reading the entire TRC (Greg Loew Panel) report and many other documents. Each member traveled at least 75,000 miles, read about 3000 pages, and had continuing interactions with the concerned community. Each had to put aside a significant part of their regular jobs. Attendance at the meetings was almost 100% and they left no stone unturned in shedding light on their challenge.

The committee report and executive summary as well as Barish's presentation to ICFA can be found through a link on the interactions.org web site.

1.3.2 Executive Summary of the International Technology Recommendation Panel (ITRP) Report

1.3.2.1 Introduction

Particle physics stands at the threshold of discovery. The standard model gives a precise and quantitative description of the interactions of quarks and leptons. Its predictions have been confirmed by hundreds of experimental measurements. Nevertheless, experiments at accelerators and observations of the cosmos point to phenomena that cannot be explained by the standard model. Dark matter, dark energy and neutrino masses all require new physics beyond present understanding. Exploring this new frontier will be the task of twenty-first century particle physics.

The essential first step is to find the Higgs boson, or whatever mechanism takes its place. The Higgs is a revolutionary new form of matter whose interactions give mass to the elementary particles. If it exists, the Higgs should be discovered at the CERN LHC, but measuring its properties with precision will require a TeV-scale electron-positron linear collider. Beyond the Higgs, strong arguments suggest that the TeV scale will be fertile ground for discovery. The LHC will open this new territory, and a TeV-scale

linear collider will be necessary to explore it in detail. Higher precision leads to greater understanding and discovery. For these reasons, the global particle physics community has endorsed such a linear collider as the next major step in the field. The case for its construction is firm.

During the past decade, dedicated and successful work by several research groups has demonstrated that a linear collider can be built and reliably operated. There are two competing designs. One, developed by the TESLA collaboration, accelerates beams in 1.3 GHz (L-band) superconducting cavities. The other, a result of joint research by the NLC and GLC collaborations, accelerates beams using 11.4 GHz (X-band) room temperature copper structures. Both R&D programs have verified the proofs of principle for the accelerating structures and the systems that drive them. The critical R&D steps were reviewed in the Technical Review Committee (TRC) charged by the International Committee for Future Accelerators (ICFA) to assess the technical readiness of these designs. The essential R&D milestones identified by the TRC in its 2003 report have now been met.

In 2004, ICFA formed the International Technology Recommendation Panel (ITRP) to evaluate the two technologies and to recommend a single choice on which to base the linear collider. Our panel met six times from January to August 2004 to hear presentations by the proponents of the two projects, gather input from the wider community, evaluate the information and prepare our recommendation. We requested responses from the proponents to an extensive set of questions. We based our decision on a set of criteria that addressed scientific, technical, cost, schedule, operability issues for each technology, as well as their wider impacts on the field and beyond.

1.3.2.2 Recommendation and rationale

The ITRP charge specified a set of design goals for the linear collider. We found that both technologies can achieve the goals presented in the charge. Both have been pursued by dedicated and talented collaborations of physicists and engineers from around the world. Each collaboration has made important contributions that will prove essential to the successful realization of the linear collider.

The details of our assessment are presented in the body of this report. On the basis of that assessment, we recommend that the linear collider be based on superconducting rf technology. This recommendation is made with the understanding that we are recommending a technology, not a design. We expect the final design to be developed by a team drawn from the combined warm and cold linear collider communities, taking full advantage of the experience and expertise of both.

Our evaluation process focused on the major acceleration and beam transfer elements of each design. We also examined other critical components, including the damping rings and the positron source. We found that both technologies can achieve the goals presented in the charge. Each had considerable strengths.

The warm technology allows a greater energy reach for a fixed length, and the damping rings and positron source are simpler. The panel acknowledged that these are strong arguments in favor of the warm technology. One member (Sugawara) felt that they were decisive.

The superconducting technology has features, some of which follow from the low rf frequency, that the Panel considered attractive and that will facilitate the future design:

- The large cavity aperture and long bunch interval simplify operations, reduce the sensitivity to ground motion, permit inter-bunch feedback, and may enable increased beam current.
- The main linac and rf systems, the single largest technical cost elements, are of comparatively lower risk.
- The construction of the superconducting XFEL free electron laser will provide prototypes and test many aspects of the linac.
- The industrialization of most major components of the linac is underway.
- The use of superconducting cavities significantly reduces power consumption.

Both technologies have wider impact beyond particle physics. The superconducting rf technology has applications in other fields of accelerator-based research, while the X-band rf technology has applications in medicine and other areas.

1.3.2.3 The next steps

The choice of the technology should enable the project to move forward rapidly. This will require the engagement of both cold and warm proponents, augmented by new teams from laboratories and universities in all regions. The experience gained from the Stanford Linear Collider and Final Focus Test Beam at SLAC, the Accelerator Test Facility at KEK, and the TESLA Test Facility at DESY will be crucial in the design, construction and operation of the machine. The range of systems from sources to beam delivery is so extensive that an optimized design can only emerge by pooling the expertise of all participants.

The machine will be designed to begin operation at 500 GeV, with a capability for an upgrade to about 1 TeV, as the physics requires. This capability is an essential feature of the design. Therefore we urge that part of the global R&D and design effort be focused on increasing the ultimate collider energy to the maximum extent feasible.

We endorse the effort now underway to establish an international model for the design, engineering, industrialization and construction of the linear collider. Formulating that model in consultation with governments is an immediate priority. Strong central management will be critical from the beginning.

A TeV scale electron-positron linear collider is an essential part of a grand adventure that will provide new insights into the structure of space, time, matter and energy. We believe that the technology for achieving this goal is now in hand, and that the prospects for its success are extraordinarily bright.

1.3.3 Links to International Linear Collider websites

ICFA home page	http://www.fnal.gov/directorate/icfa/icfa_home.html
ITRP home - reports, talks	http://www.ligo.caltech.edu/~skammer/ITRP_Home.htm
ILCSC home page	http://www.fnal.gov/directorate/icfa/International_ILCSC.html
Interactions.Org ILC	http://www.interactions.org/linearcollider/

2 The Beam-beam Interaction

2.1 Symplectic Treatment of a Finite Crossing Angle in the Beam-Beam Collision

Yunhai Cai, SLAC
mail to: yunhai@slac.stanford.edu

Abstract

We introduce a symplectic method to handle a large and finite crossing angle in the beam-beam interaction. This method has been implemented in a parallel computer program to simulate three-dimensional effects in the beam-beam interaction. Our simulation results are compared with the known analytical solutions, the simulations using the Lorentz boost and experimental observations.

2.1.1 Introduction

The beam-beam effects due to a vertical crossing angle were experimentally and theoretically investigated by Piwinski [1]. He showed that the crossing angle coupled the transverse and longitudinal oscillations and therefore excited the synchrotron-betatron resonances which lead to the degradation of luminosity. Since the horizontal beam size is naturally much larger than the vertical size in e^+e^- storage rings, the allowed crossing angle in the horizontal plane may well be much larger than the one in the vertical plane. This possibility was systematically studied by Hirata [2] who introduced a transformation called “Lorentz Boost". Using the boost, he simulated the dynamical effects due to a large crossing angle within the strong-weak approximation. His work has established the feasibility of using a crossing angle as a realistic scheme to separate the colliding beams near the interaction point (IP) in e^+e^- storage rings.

Since the birth of a new generation of high-luminosity e^+e^- colliders [3,4,5], the beam-beam collision with a finite crossing angle in the horizontal plane has become a reality [4,5]. The positive and successful experience of these modern accelerators has prompted us to adopt the crossing scheme into the designs and upgrades of the e^+e^- storage rings [6] and the hadron colliders [7,8].

Based on these recent developments, it is clear that the beam physics related to the crossing angle has become critically important. A concern regrading the Lorentz boost is: the violation of the symplecticity because of the explicit use of the Lorentz boost in its composition. It is well known that the violation of symplecticity may cause artificial growth of emittance [9]. Of course, it was pointed out by Hirata in his paper [2] and recently by Ohmi [10] that the net effect is symplectic if its inverse is used after the beam-beam kick.

In this letter, we continue along the work of Piwinski and develop a geometrical method to treat exactly a collision without use of the Lerentz boost for a finite crossing angle. The symplecticity is preserved throughout the collision process.

2.1.2 Geometrical transformations

Let's use $x, p_x, y, p_y, \delta, l$ as the canonical coordinates of a charge particle, where x, y are the transverse displacements, δ is the relative momentum deviation and l is the path length relative to the synchronous particle. When two beams collide with a horizontal crossing angle, we need a transformation that rotates the particles in a single slice ($s = 0$) to the head-on frame ($s^* = 0$) as illustrated in Fig 1. It is clear that the axis of the rotation is the y axis. It is well known [11] that, in the context of single-particle dynamics, this transformation can be generated by the Lie operator: $R_y(\phi) = \exp(: xp_s :)\phi$, where $p_s = \sqrt{(1+\delta)^2 - p_x^2 - p_y^2}$

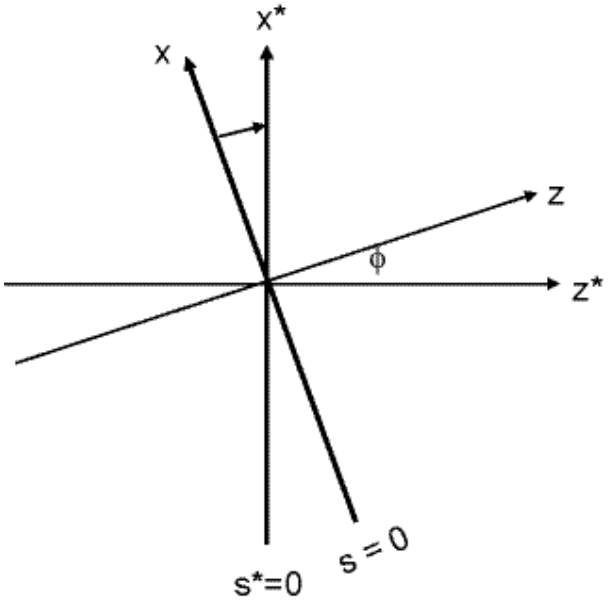

Figure 1. A rotational transformation.

The explicit transformation can be obtained by solving the Hamiltonian's equations with $H = -xp_s$ and ϕ as the independent variable. It can be written as follows,

$$
\begin{aligned}
x^* &= \frac{xp_s}{\cos\phi(p_s - p_x \tan\phi)}, \\
p_x^* &= p_x \cos\phi + p_s \sin\phi, \\
y^* &= y + \frac{xp_y \tan\phi}{(p_s - p_x \tan\phi)}, \\
p_y^* &= p_y, \\
\delta^* &= \delta, \\
l^* &= l + \frac{x(1+\delta)\tan\phi}{(p_s - p_x \tan\phi)}.
\end{aligned} \tag{1}
$$

Since it is the exact solution of the Hamiltonian's equation, it is symplectic. To treat a three-dimensional beam, there are other coordinate transformation needed. They are the horizontal displacement $\mathrm{D}_x(\delta x) = \exp(: p_x :)\delta x$ and the drift operator $\mathrm{D}_z(\delta s) = \exp(: p_s :)\delta s$.

2.1.3 Collision

For every collision, the macro particles are cast into the slices according to their longitudinal positions. Since the beam distributions are dynamically evolved during the collision, the sequence of the colliding slices is identical to the time sequence.

For a given pair of colliding slices at $z^{\pm} = -l^{\pm}$, we need to compute where the collision actually occurs: $s^{\pm} = (z^{\pm} - z^{\mp})/2$ and drift the particles in the slices to the collision point by the operator $\mathrm{D}_z^{\pm}(s^{\pm}) = \mathrm{D}_z(s^{\pm})$ so that the hourglass and phase-average effects due to a finite bunch length are properly included in the simulation.

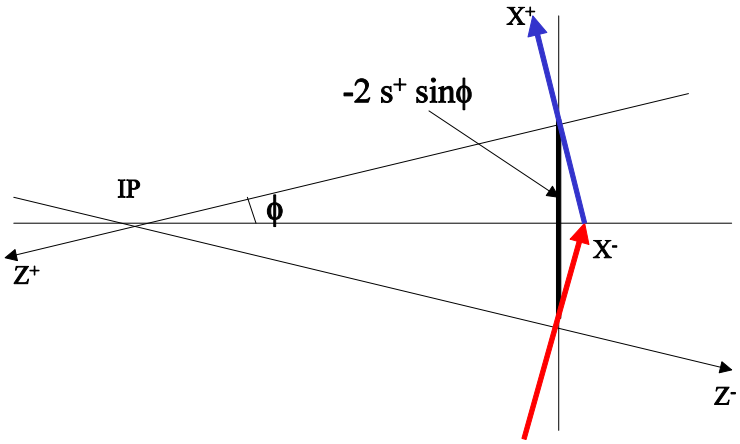

Figure 2. Two slices of beam colliding at their actual collision point with an angle 2ϕ .

As illustrated in Fig. 2, if there is a crossing angle, we need to make the transformation $R_y^{\pm}(\phi) = R_y(\pm\phi)$. After the rotations, there is still a displacement of two coordinate systems in the horizontal plane as shown in Fig 2; we use operator: $D_x^{\pm}(s^{\pm}, \phi) = D_x(-2s^{\pm}\sin\phi)$ to transform the coordinates of the particles to the coordinate system in which the beam-beam force from the opposing beam is calculated so that the force can be applied to the particles. After the beam-beam kick, we applied the reverse operation in the inverted order to move the particles in the slice back inside the beam.

The whole process can be summarized and written as

$$T^{\pm}(s^{\pm}, \phi) \cdot O_{BB}^{\mp}(x^{\pm}, y^{\pm}, \phi) \cdot T^{\pm}(s^{\pm}, \phi)^{-1}, \tag{2}$$

where

$$T^{\pm}(s^{\pm}, \phi) = D_z^{\pm}(s^{\pm}) \cdot R_y^{\pm}(\phi) \cdot D_x^{\pm}(s^{\pm}, \phi), \tag{3}$$

and $O_{BB}^{\mp}(x^{\pm}, y^{\pm}, \phi)$ represents the operator for the beam-beam kick.

Here we use the following convention in the map operation: The operator on the left acts on function of the canonical coordinates first and the dot represents the concatenation of two maps.

Using the particle distributions at the collision point, we obtain the beam-beam force by solving the two-dimensional Poisson equation [12]. Because of the crossing angle ϕ, the integrated beam-beam kick by a slice needs to be modified to

$$\begin{aligned}
\Delta p_x^{\pm} &= -\frac{e}{E_0^{\pm}} \cos\phi \int_{slice} E_x^{\mp} ds, \\
\Delta p_y^{\pm} &= -\frac{e}{E_0^{\pm}} \int_{slice} E_y^{\mp} ds, \\
\Delta \delta^{\pm} &= -\frac{e}{E_0^{\pm}} \sin\phi \int_{slice} E_x^{\mp} ds,
\end{aligned} \tag{4}$$

where E_x and E_y are the transverse electric fields and E_0 is the energy of the synchronous particle. Here we have assumed that the particles are ultra-relativistic and $E_0 = cp_0$.

2.1.4 Geometrical effect

The geometric degradation of luminosity due to the hourglass effect and the crossing angle is given by Hirata [2]

$$\begin{aligned}
R_L &= \frac{L}{L_0} = \sqrt{\frac{2}{\pi}} a e^b K_0(b), \\
a &= \frac{\sigma_y^*}{\sqrt{2}\sigma_z^* \sigma_{p_y}^*}, b = a^2[1 + (\frac{\sigma_z^*}{\sigma_x^*} \tan\phi)^2],
\end{aligned} \tag{5}$$

where L and L_0 is the luminosity with or without the hourglass effects and crossing angle and K_0 is a modified Bessel function.

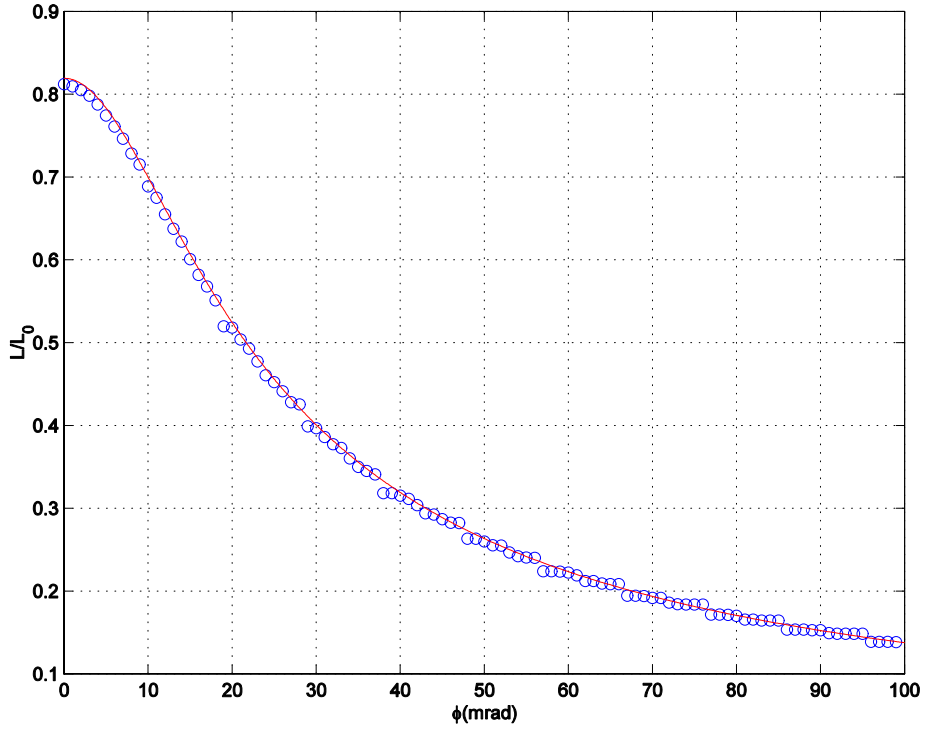

Figure 3. The circles represent the simulation results using 50,000 macro particles on a mesh of $128\times256\times31$ and the solid is the plot of Eq. (6) with $\sigma_x^* = 110.84$ μm, $\sigma_y^* = 1.16$ μm, $\sigma_{p_y}^* = 181.14$ μrad, and $\sigma_z^* = 7.9$ mm.

Since this is a purely geometrical and single-turn effect, we do not need to compute the electric and magnetic field during the collision. The simulated luminosity is calculated from the summation of overlapping beam distributions on the transverse head-on grids over all possible pairs of the colliding slice. The result of the simulation is shown in Fig. 3 for the symmetrized KEKB parameters. The excellent agreement between the simulation and the analytical analysis over a large range of the crossing angle provides an independent check of the accuracy of using these geometrical transformations.

2.1.5 Parallel computing

To achieve the required numerical convergence in the three-dimensional simulation forces the use of parallel supercomputers. One of the most important aspects of parallel computing is how to minimize the communication among processors. Each application may have a different optimal solution. For beam-beam simulations, we have developed an efficient strategy utilizing dual processors. Macro particles are evenly distributed across many processors. The processors are divided into two groups, one for the positron beam and the other for the electrons. Before the collision, the beam distribution on the grid is summed within each group, and the resulting distribution is distributed back to all processors in the group. Then the total distribution is exchanged between the groups. That allows us to solve the Poisson equation and compute the force on the macro particles in every local processor.

In this scheme, the macro particles always remain confined to the same computing processor. The division into two groups essentially allows us to double the speed without much penalty.

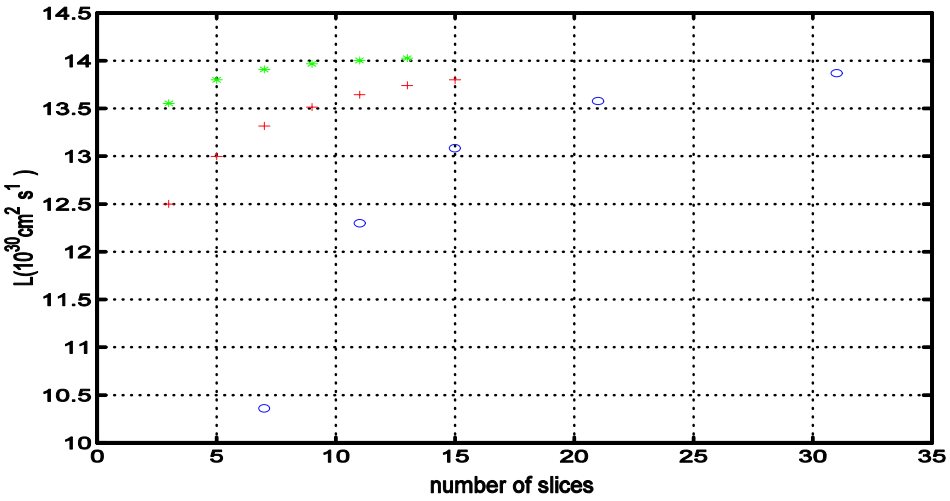

Figure 4. Simulated luminosity as a function of number of longitudinal slices. The circles represent the results of using equal-spacing slices, the crosses for equal-area slices, and the starts for equal-area slices with linear interpolation between the slices.

A linear and stochastic map [13] that includes the betatron and synchrotron oscillations, the radiation damping, and the quantum excitation is used in the arc to track the particles. The map also properly gives the effects of the dynamical beta and dynamical emittance [14] near the horizontal half integer.

Using 32 processors on a parallel computer at NERSC [15], we are able to achieve the required convergence with five linearly interpolated [10] and equal-strength slices [13] as shown in Fig 4. For a typical simulation, we use 160,000 macro particles for each beam with a mesh $128\times128\times5$. The area of the mesh has to be large enough to retain the particles in the tail of beam, especially in the vertical plane. In practice, we choose it so that the accumulated loss of the particles beyond the mesh during the whole run is less than a few percent even at the peak of the beam intensities. To reach equilibrium of the beam distributions, each simulation takes about eight hours on the supercomputer.

2.1.6 Dynamical effect

The dynamical degradation of the luminosity from a finite crossing angle can be more severe than the geometrical reduction because of the synchro-betatron coupling introduced from the angle. To study this effect, a simulation is carried out for the present parameters, tabulated in Table 1, at KEKB to benchmark against a well-known code [16] based on Hirata's work. The results of the two simulations are shown in Fig. 5.

Table 1. The present parameters of KEKB. The crossing angle is $\pm 11 mrad$.

Parameter	Description	e^+	e^-
E (Gev)	beam energy	3.5	8.0
$N\,(10^{10})$	bunch population	7.36	5.28
β_x^* (cm)	beta x at the IP	59.0	58.0
β_y^* (mm)	beta y at the IP	5.8	7.0
$[\text{epsilon}]_x$(nm-rad)	emittance x	18.0	24.0
$[\text{epsilon}]_y$(nm-rad)	emittance y	0.18	0.24
ν_x	x tune	0.506	0.513
ν_y	y tune	0.545	0.586
ν_s	z tune	0.0249	0.0207
σ_z (mm)	bunch length	8.7	7.1
$\sigma_p\,(10^{-4})$	energy spread	7.26	6.67
τ_t (turn)	x, y damping time	4000	4000
τ_s (turn)	z damping time	2000	2000

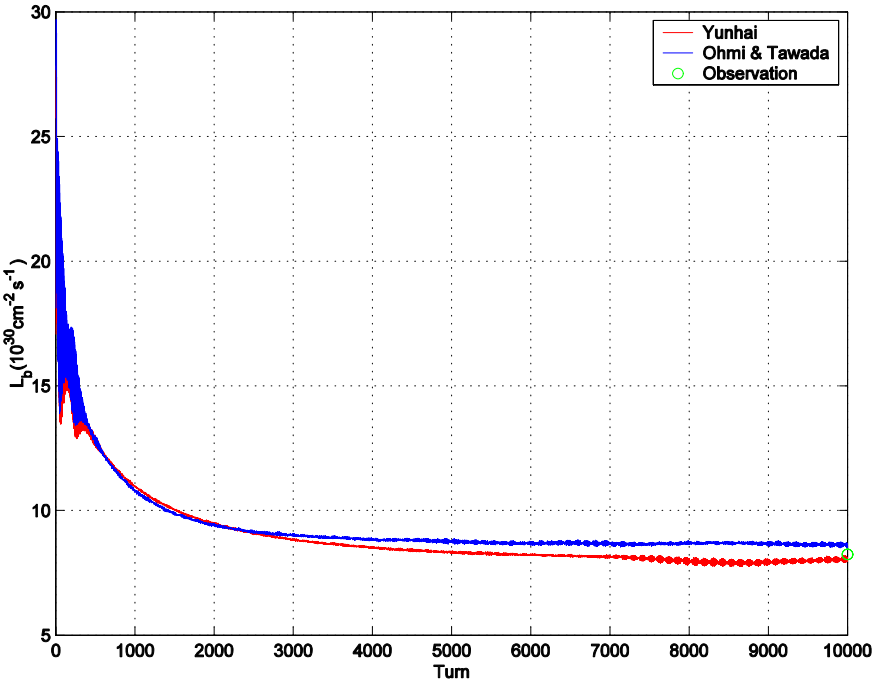

Figure 5. The simulated bunch luminosity is compared with the result obtained by Ohmi and Tawada for the present KEKB parameters at the peak beam currents and the measurement on May 3, 2003.

The equilibrium luminosities obtained from the simulations and the measurement agree within 5%. The measured luminosity is nearly at the middle of the two simulations. The equilibrium beam sizes agree within a few percentages between the two codes. At the peak beam intensities, the total luminosity reduction due to the crossing angle of $\phi = \pm 11$ mrad is 58%, which is significantly higher than its geometric degradation 17%.

The success of reaching its design luminosity at KEKB has clearly demonstrates many advantages of the design with the crossing angle. Still, the simulation shows that its luminosity could be doubled if one simply compensates the crossing angle with crab cavities [17]. However, this result also implies that the head-on collision has a potential to produce twice the luminosity at extremely high intensities of beam compared to the collision with an angle.

In additional to these simulations, we also benchmark the two codes at the current PEP-II working point and the super KEKB parameters. The results in agreement or disagreement are similar. Since they are all head-on collisions, the results are not shown in this letter.

2.1.7 Discussions

We have demonstrated that this geometrical method works just as well as the traditional method using the Lorentz boost in e^+e^- storage rings. Since the method is based entirely on the Lie operators during the collision, it is manifestly sympletic. Moreover, it has a geometric interpretation at each step of the operation.

2.1.8 Acknowledgments

We gratefully thank Kazuhito Ohmi and Masafumi Tawada for providing the KEKB parameters and their simulation results. We would like also to thank Robert Ryne for his generosity in providing the computing resource at NERSC. This work was supported by the U.S. Department of Energy, under Contract No. DE–AC02–76SF00515.

2.1.9 References

1. A. Piwinski, “Satellite resonances due to beam-beam interaction", 1977 Particle Accel. Conf., IEEE Trans. V. NS-24, No.3 p.1408 (1977).
2. K. Hirata, “Analysis of beam-beam interactions with a large crossing angle", Phys. Rev. Lett. 2228 (1995).
3. “PEP-II conceptual design report", SLAC-418, LBL-PUB-3579, June (1993).
4. “KEKB B-factory design report", KEK-Report-95-7, (1995).
5. G. Vignola *el al*, 1996 Erupean Particle Accel. Conf., p.22 (1996).
6. “BEPCII design report", IHEP-AC-Report/2002-01, BEPCII-Report/2002-01, May (2002).
7. F. Ruggiero and F. Zimmermann, “Luminosity optimization near the beam-beam limit by increasing bunch length or crossing angle", Phys. Rev. ST Accel. Beams , 061001 (2002).
8. “Run II handbook", Fermilab Technical Design Report, November (1996).

9. D. Douglas, E. Forest, and R. V. Servranckx, “A method to render second order beam optics programs symplectic," IEEE Trans. Nucl. Sci. 2279 (1985).
10. K. Ohmi, *et al*, “Study of Beam-Beam Interactions with or without Crossing Angle," KEK-PREPRINT-2004-17, May 2004, SLAC-PUB-10532.
11. E. Forest, M. F. Reusch, D. L. Bruhwiler, and A. Amiry, “The Correct Local Description for Tracking in Rings," Part. Accel. 66 (1994).
12. Y. Cai, A. W. Chao, S. I. Tzenov, and T. Tajima, “Simulation of the beam-beam effects in e^+e^- storage rings with a method of reducing the region of mesh," Phys. Rev. ST Accel. Beams , 011001 (2001).
13. K. Hirata, H. Moshammer, and F. Ruggiero, “A symplectic beam-beam interaction with energy change," Particle Accelerator, , 205 (1993).
14. K. Hirata and F. Ruggiero, “Treatment of Radiation in electron storage rings," LEP notes 661, August 8, (1988).
15. The National Energy Research Scientific Computing Center supported by the Office of Science of the U.S. Department of Energy.
16. K. Ohmi, “Simulation of beam-beam effects in a circular e^+e^- collider," Phys. Rev. E , 7287 (2000).
17. K. Oide and K. Yokoya, “Beam-beam collision scheme for storage-ring collider," Phys. Rev. A , 315 (1989).

2.2 Strong-strong beam-beam simulation on parallel computer

Ji Qiang, LBNL
mail to: jqiang@lbl.gov

2.2.1 Introduction

The beam-beam interaction puts a strong limit on the luminosity of the high energy storage ring colliders. At the interaction points, the electromagnetic fields generated by

one beam focus or defocus the opposite beam. This can cause beam blowup and a reduction of luminosity. An accurate simulation of the beam-beam interaction is needed to help optimize the luminosity in high energy colliders.

Macroparticle tracking provides an invaluable tool for the study of beam-beam interactions. In this approach, a number of simulation particles (“macroparticles”) are used with the same charge-to-mass ratio as the real particles. Outside the interaction region, the macroparticles are transported through the simulated lattice using transfer maps associated with external elements, radiation damping, and quantum excitation. At the interaction point, the electromagnetic fields from the beams are calculated and applied to the particles of the opposing beam.

The soft Gaussian approximation is sometimes used to obtain the electromagnetic fields of the beams at the collision point [1-3]. While this approximation has the advantage of computational speed, it is not self-consistent because it assumes a Gaussian distribution for the macroparticles even when the actual distribution might differ substantially from the Gaussian shape. To take into account the effects of the beam distribution self-consistently, one has to solve the Poisson equation numerically during each collision for the actual macroparticle distribution at that instant.

A number of methods have been used to solve the Poisson equation. The five-point finite difference method with Fourier analysis and cyclic reduction (FACR) has been used by Krishnagopal [4] and Cai et al. [5]. This method solves the Poisson equation efficiently with finite domain boundary conditions. For the open boundary conditions, which are appropriate in typical beam-beam simulations, the method requires finding an effective boundary condition on the problem boundary; this can be computationally expensive. In addition, this method is not efficient to handle the case with two widely separated beams, where the domain of the source particles (particle domain) and the domain of the electric field (field domain) are different. Another method based on the fast multipole expansion has been used by Herr et al. [6] to solve the Poisson equation. In this method, the computational cost scales linearly with the number of particles or with the number of total mesh points for the open boundary condition. The efficiency of this method is independent of the distribution of the source particles and the field domain, which makes it suitable to handle the situation with two separated beams. However, this method is an approximate algorithm in a sense that the accuracy of the expansion depends on the radius of convergence. The computational speed depends on the number of polynomials required in the multipole expansion.

The most widely used method to solve the Poisson equation in beam-beam simulations is the Green function method with fast Fourier transform (FFT). This method uses an FFT to calculate the cyclic summation on a doubled computational grid [7-11]. By defining a new shifted integrated Green function, this method can handle the separated beams, and beams with large aspect ratio. During the beam-beam interaction, when the bunch length is large compared with the beta function value or the beam-beam forces are strong, finite bunch length effects are not negligible. In this case, a multiple slice model has to be used. The computational cost scales as the square of the number of slices. For a hadron collider with tiny radiation damping, it is required to track the beams for many millions of turns to study the dynamics on the time scale of the lifetime of the beams. To study the beam-beam interaction fully self-consistently for both beams (i.e. a "strong-strong" formulation), and to include all the physical processes of long range off-centroid interactions, finite beam bunch length effects, and crossing angle collisions, requires computational resources far beyond the capability of current serial computers. A parallel beam-beam simulation model, with both weak-strong and strong-strong capabilities, that can simulate these physical processes accurately using high performance computers has been developed at Lawrence Berkeley National Laboratory [12], and is briefly described below along with a few applications.

2.2.2 Computational Model

In the computational model of strong-strong beam simulation, each charged particle is characterized by its charge, mass, and phase space coordinates (x, p_x, y, p_y, Δz, $\Delta p / p_0$). Here, the independent variable, s, is the arc length along a reference trajectory inside the accelerator, $p_{\{x,y\}}$ is the transverse momentum normalized by the total momentum of a reference particle ($p_0 = E_0/c$), $\Delta z = s - ct(s)$ with c the speed of light, $\Delta p = |p| - p_0$ with p_0 the absolute momentum value of the reference particle. The beam-beam forces, under the relativistic limit, can be obtained from the solution of the two dimensional Poisson equation. The effect of finite bunch length is included using a multiple slice model. In this model, each beam bunch is divided into a number of slices along the longitudinal direction in the moving frame. Each slice contains nearly the

same number of particles at different longitudinal locations z. The collision point between two opposite slices is determined and the particles are moved to the collision point through a drift. At the collision point, the slopes of the particles are updated using the beam-beam electromagnetic forces at the collision point following

$$p_{x_2}^{new} = p_{x_2} + \frac{2q_1q_2N_1}{\gamma_2 4\pi\varepsilon_0 m_2 c^2} E_{x_1} \tag{1}$$

$$p_{y_2}^{new} = p_{y_2} + \frac{2q_1q_2N_1}{\gamma_2 4\pi\varepsilon_0 m_2 c^2} E_{y_1} \tag{2}$$

In the above equations, the subscripts 1 and 2 refer to each of the two beams. The corresponding equations for the other beam are obtained from the above by exchanging
1 and 2. The other symbols have the following meaning: $\gamma = 1/(1-\beta^2)^{1/2}$, $\beta_i = v_i/c$, i = x,y,z, c is the speed of light, ε_0 is the vacuum permittivity, q is the charge of the particle, m is the rest mass of the particle, N is the number of particles in a bunch, and E_x and E_y are the transverse electric fields generated by the opposite moving beam.

The solution of Poisson's equation can be written as

$$\phi(x,y) = \frac{1}{2\pi\varepsilon_0}\int G(x,\bar{x},y,\bar{y})\rho(\bar{x},\bar{y})\, d\bar{x}\bar{y} \tag{3}$$

where G is the Green function and ρ is the accumulated charge density distribution within a slice. For the case of transverse open boundary conditions, the Green function is given by:

$$G(x,\bar{x},y,\bar{y}) = -\frac{1}{2}\ln((x-\bar{x})^2 + (y-\bar{y})^2) \tag{4}$$

The calculation of the above convolution using a direct summation is not efficient and scales as the square of the total number of computational mesh points. Fortunately, the direct summation can be replaced by a cyclic summation in a double-gridded computational domain. The cyclic summation can be done very efficiently using a discrete fast Fourier transform (FFT) [13].

In the original FFT-based algorithm, the particle source domain and the electric field domain are contained in the same computational domain. Here, the particle domain is the configuration space containing the charged particles, and the field domain is the space where the electric field is generated by the charged particles. In the beam-beam interaction, the two opposite moving beams might not overlap with each other, e.g. in the case of parasitic collisions. To apply Hockney's algorithm directly requires the computational domain to contain both the particle domain and the field domain, i.e. both beams must be fully contained in the common domain. Since there is a large empty space between two separated beams, containing both beams in one computational domain results in poor spatial resolution. This is also computationally inefficient because the electric fields in the empty space between the two beams are not used. To avoid this problem, we have defined a shifted Green function as

$$G_s(x,\bar{x},y,\bar{y}) = -\frac{1}{2}\ln((x_c + x - \bar{x})^2 + (y_c + y - \bar{y})^2) \tag{5}$$

where x_c and y_c are the center coordinates of the field domain. Using the shifted Green function, the computational domain contains the larger one of the two separated beams. This saves the computational cost and also improves the numerical accuracy of the solution.

When the colliding beams have large horizontal (x) to vertical (y) aspect ratio, the straightforward use of the Green function at each mesh point is not efficient since it requires a large number of mesh points along the longer direction in order to get sufficient resolution for the Green function along that direction. An alternative way is to define an effective Green function as

$$G_s^{\,eff} = \int_{x_{i'}+h_x/2}^{x_{i'}-h_x/2} dx' \int_{y_{j'}+h_y/2}^{y_{j'}-h_y/2} dy'\, G_s(x_i - x', y_j - y') \qquad (6)$$

The use of the effective Green function has been found to be valuable for modeling high aspect ratio beams [8,12]

Lastly, the effects of external focusing fields can be simulated, in the small-amplitude approximation, by a one-turn linear map. In our case, we include in this map the effects from linear machine chromaticity. The effects of radiation damping and quantum excitation can be represented using a localized stochastic map [14]. When two beams collide at a finite angle, a transformation is used to change the crossing angle collision in the laboratory frame into a head-on collision in the boosted moving frame [15-16].

2.2.3 Parallel Implementation

In the parallel implementation, we have used a particle-field decomposition method. In this approach, each processor possesses the same number of particles and the same number of computational grid points, i.e, the same size of spatial subdomain. Fig. 1 shows a schematic plot of the particle-field decomposition among three processors.

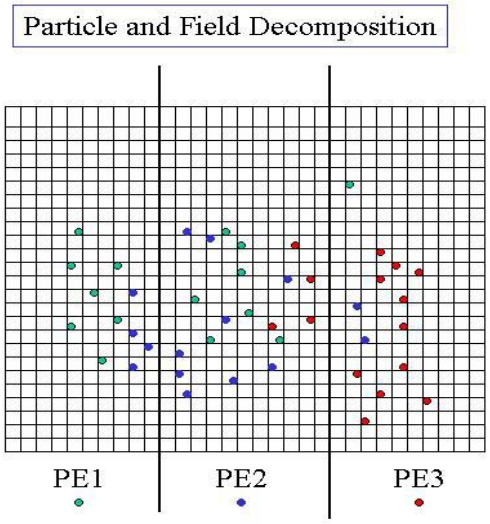

Figure 1: A schematic plot of particle-field decomposition

The global computational mesh is uniformly distributed among the processors. The spatial coordinates of the particles on each processor might not stay within the spatial mesh domain of that processor. In the process of solving the Poisson equation, the particles are deposited onto the computational grid to obtain the charge density distribution. For the particles with spatial positions outside the local subdomain, an

auxiliary computational grid is used to store the charge density. After the deposition, the charge density stored on the auxiliary grid is sent to the processor containing that subdomain. With charge density local to each processor, the Poisson equation is solved in parallel on a local subdomain using a Green function method. The solution of the electric potential on the local subdomain is sent to all processors. With the electric potential on each processor, the electric field is calculated on the grid and interpolated onto individual particles of the opposite beam. The particles are advanced using the electromagnetic field and the external maps. Since each processor contains the same number of particles, the work of this process is also well balanced among processors. In the particle-field decomposition approach, the volume of communication is proportional to the number of computational grid points. In the domain decomposition approach, it is proportional to the number of particles that cross domain boundaries; this number can be close to the total number of particles due to the particle movement associated with the one-turn map. Since, in the study of beam-beam interactions, the number of particles is much larger than the number of computational grid points, e.g. typically10^6 versus 10^4, the particle-field decomposition approach can significantly reduce the communication cost in the simulation. This algorithm is more scalable than domain decomposition or particle decomposition when applied to beam-beam simulations [12].

2.2.4 Applications

The computational program described in the preceding sections has been applied to the study of beam-beam interactions at RHIC, LHC, Tevatron, PEP-II, and KEKB [10, 17-18]. In the following, we will present two examples of the strong-strong simulations, one for LHC and one for PEP-II.

A "sweeping beam detector" has been proposed as a device to monitor and to optimize the luminosity at the LHC. In this scheme, one of the beams is deliberately made to rotate about a fixed axis as it collides with the opposite beam. Previous beam-beam simulations, carried out up to 100,000 turns, suggest that there is little or no emittance growth for the nominal design parameters [10]. This corresponds to about nine seconds of machine operation time. In order to be measurable in real machine operation, in this example, we show the emittance evolution up to one million turns from the strong-strong beam-beam simulation corresponding to about 90 seconds of machine time. For such a long time simulation, the emittance growth driven by the numerical collisionality is no longer negligible. To quantify this purely computational effect, we have varied the number of macroparticles per beam from $2x10^5$ to $2x10^6$. Fig. 1 shows the averaged emittance growth after one million turns as a function of number of macroparticles.

The real emittance growth after one million turns can be estimated from the extrapolation, which gives about 0.05% emittance growth. It can be seen that for a quarter million macroparticles, the numerical emittance growth is much higher than the real emittance growth.

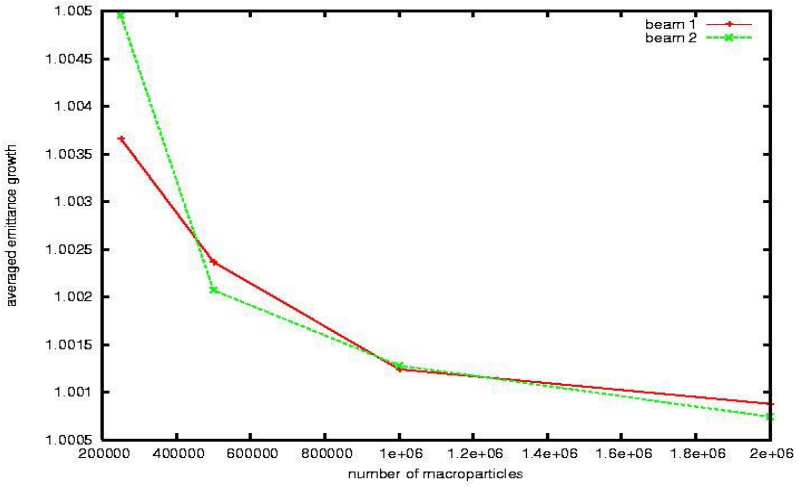

Figure 2: Emittance growth after one million turns as a function of the number of macroparticles for the LHC sweeping luminosity monitor.

In the strong-strong beam-beam simulation, when the beam-beam forces are weak and the bunch length is small compared with the beta function at the collision point, finite bunch length effects can be neglected and the simulation can be done using a single slice for each beam. In most lepton colliders, the beam-beam forces are relatively strong and the bunch length is not small compared with the beta function value. In this case, a multiple slice model has to be used for each beam in the strong-strong beam-beam simulation. Fig. 3 shows luminosity as a function of turns using a single slice and 20 slices for a strong-strong beam-beam simulation for PEP-II. It can be seen that there is a significant difference in the simulated luminosity after several damping times. This suggests that multiple slices should be used in order to accurately predict the luminosity of a lepton machine like PEP-II.

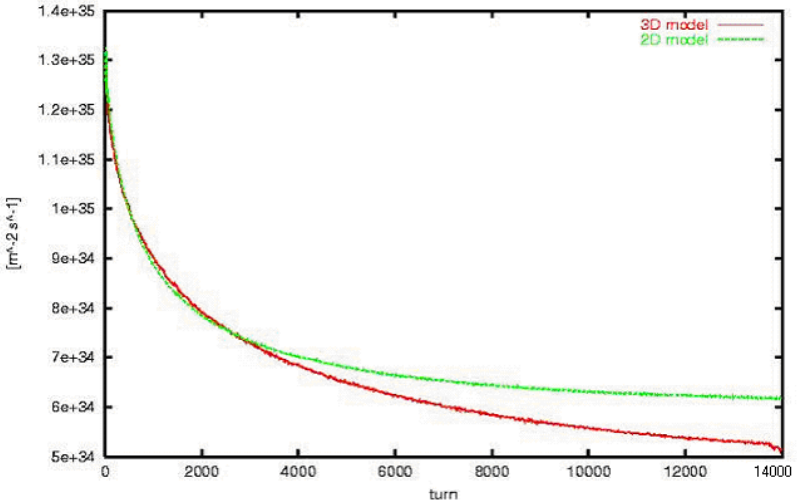

Figure 3: Single collision luminosity as a function of turns at PEP-II predicted using 1 slice (2d model) and 20 slices (3d model).

2.2.5 Acknowledgements

We would like to thank Drs. R. Ryne and M. Furman for helpful discussions and manuscript reading. We also thank Dr. Y. Cai for the PEP-II parameters used in the simulation. This research used resources of the National Energy Research Scientific Computing Center (NERSC) and the resources of the Center for Computational Sciences at Oak Ridge National Laboratory. Some of the computational work for this project was done on the LBL/NERSC Alvarez Cluster, an 80 node Pentium III Myrinet cluster. This work was supported by the U. S. Department of Energy under Contract no. DE-AC03-76SF00098, and by a Scientific Discovery through Advanced Computing project, "Advanced Computing for 21st Century Accelerator Science and Technology," which is supported by the US DOE/SC Office of High Energy Physics and the Office of Advanced Scientific Computing Research.

2.2.6 References

1. K. Hirata, H. Moshammer and F. Ruggiero, Particle Accelerators, vol. 40, 1993, pp. 205-228.
2. M. A. Furman, "Beam-Beam Simulations with the Gaussian Code TRS", LBNL-42669, CBP Note 272, 1999.
3. M. P. Zorzano and F. Zimmermann, Phys. Rev. Special Topics - Accel. Beams, vol. 3, April 2000, 044401.
4. S. Krishnagopal, Phys. Rev. Lett. Vol. 76, 1996, pp. 235-238.
5. Y. Cai, A. W. Chao, S. I. Tzenov, and T. Tajima, Phys. Rev. Special Topics - Accel. Beams, vol. 4, Jan. 2000, 011001.
6. W. Herr, M. P. Zorzano, and F. Jones, Phys. Rev. Special Topics - Accel. Beams, vol. 4, May 2001, 054402.
7. E. B. Anderson, T. I. Banks, J. T. Rogers, in Proceedings of the 1999 Particle Accelerator Conference, New York, 1999, pp. 1686-1688.
8. K. Ohmi, Phys. Rev. E, vol. 62, 2000, pp. 7287-7294.
9. J. Shi and D. Yao, Phys. Rev. E, vol. 62, 2000, pp.1258-1265.
10. J. Qiang, M. A. Furman, and R. D. Ryne, Phys. Rev. Special Topics - Accel. Beams, vol. 5, 2002, 104402.
11. A. Kabel, in Proceedings of the 2003 Particle Accelerator Conference, Portland, 2003, pp. 3545-3547.
12. J. Qiang, M. A. Furman, and R. D. Ryne, "A parallel particle-in-cell model for beam-beam interaction in high energy ring colliders," J. Comp. Phys. 2004 (in press).
13. R. W. Hockney and J. E. Eastwood, *Computer Simulation Using Particles* (McGraw-Hill, New York, 1985).
14. M. A. Furman, A. Zholents, T. Chen, and D. Shatilov, "Comparisons of Beam-Beam Code Simulations," CBP Tech Note-59, 1996.
15. K. Hirata, Phys. Rev. Lett., vol. 74, no. 12, March 1995, pp. 2228-2231.
16. L. H. A. Leunissen, F. Schmidt, G. Ripken, Phys. Rev. Special Topics - Accel. Beams, vol. 3, Dec. 2000, 124002.

17. J. Qiang, M. Furman, R. D. Ryne, W. Fischer, T. Sen, and M. Xiao, "Parallel strong-strong/strong-weak simulations of beam-beam interaction in hadron accelerators," in Proceedings of 29th ICFA Advanced Beam Dynamics Workshop on Beam Halo Dynamics, Diagnositics, and Collimation and Workshop on Beam-Beam Interactions, Montauk, New York, 2003, pp. 278-282.
18. K. Ohmi, M. Tawada, Y. Cai, S. Kamada, K. Oide, J. Qiang, Phys. Rev. Lett. vol. 92, 2004, 214801.

2.3 Beam-Beam Effects in the Large Hadron Collider

F. Zimmermann, CERN
mail to: frank.zimmermann@cern.ch

2.3.1 Introduction

The Large Hadron Collider (LHC) is only the 5th hadron collider coming into operation, after the CERN Intersecting Storage Rings (ISR), the CERN Super Proton Synchrotron (SPS) collider, the FNAL Tevatron, and the Relativistic Heavy Ion Collider (RHIC) at BNL. As for its predecessors, the beam-beam interaction is expected to prove one of the ultimate limits to the LHC performance. In addition, the LHC is the first hadron collider with close bunch spacing, so that despite of two separate rings, a large number of up to 120 'parasitic' or long-range collisions are encountered per turn, in addition to the 4 primary collisions at the 4 detectors. The experiments in Interaction Point (IP) 1 and 5 (ATLAS and CMS) require high luminosity and operate with a small beta function and beam size. The beta function at the other two experiments, ALICE and LHCB, is about 20 times larger, and consequently, for a similar crossing angle, the long-range collisions are less of a concern here. Besides, at ALICE the beams are separated transversely by 5σ at the main collision point. Recently updated LHC beam parameters for peak luminosity are compiled in Table 1.

Table 1: LHC design parameters with protons at top energy [1]

parameter	symbol	value
proton energy	E_b	7000 GeV
relativistic gamma	γ	7461
particles per bunch	N_b	1.15×10^{11}
number of bunches	n_b	2808
transverse normalized emittance	ε_n	3.75 μm
rms bunch length	σ_z	7.55 cm
rms beam size at IP1 & 5	σ_{xy}*	16.7 μm
rms beam size at IP2 & 8	σ_{xy}*	70.9 μm
beta at IP1 & 5	β_{xy}*	0.55 m
beta at IP2 & 8	β_{xy}*	10 m
full crossing angle at IP 1 & 5	θ	285 μrad
peak luminosity in IP 1 & 5	L	1.0×10^{34} cm^{-2} s^{-1}

Several features of the beam-beam interaction at the LHC have been intensely studied over the last couple of years. These include:

- the reduction of the dynamic aperture due to the head-on and long-range beam-beam interaction [2], together with the effect of magnet field errors of the final-triplet quadrupoles [3, 4, 5, 6,7, 8];
- the variation in orbits and tunes along the bunch trains, in particular the differences between regular bunches and so-called PACMAN bunches [9], i.e., bunches at the start or end of a train, which do not experience the full number of long-range collisions (due to the filling scheme and the asymmetric location of one experiment, only about of half the bunches in the LHC are 'regular') [10, 11, 12];
- the choice of the crossing planes at the various IPs [10, 13, 14];
- the possibility of compensating the effect of long-range collisions by electromagnetic lenses and pertinent experimental studies at the SPS [15, 16, 17, 18, 19, 20];
- the effect of ground motion [21, 22, 23, 24];
- the excitation of synchro-betatron resonances due to crossing angle and spurious dispersion [25];
- halo generation [26] and long-term emittance growth [27, 28, 29, 30, 14];
- the possible loss of Landau damping in the collision of two equally strong beams, and its restoration by multiple IPs, long-range effects, synchrotron motion, unequal tunes, etc. [31, 32, 33, 34, 35, 36, 37, 38, 28, 39, 40, 41, 42];
- the alternative paths towards higher luminosity, involving either shorter Gaussian, or longer uniform bunches or superbunches [43, 44] and/or crab cavities [45, 46, 14].

Below I describe a few of these issues in greater detail.

2.3.2 Tune Shift

Beam-beam tune shifts at hadron colliders have so far been limited to values about an order magnitude lower than those at lepton colliders. For a short round bunch without crossing angle, the head-on beam-beam tune shift and tune spread from one IP are characterized by the parameter

$$\xi_{HO} \equiv \frac{N_b r_p}{4\pi\gamma\varepsilon_{x,y}},$$

where N_b is the bunch population, r_p the classical proton radius, and $\varepsilon_{x,y}$ the geometric rms emtitance.

The total tune shift is roughly the sum of the ξ_{HO}'s from the different IPs (here ignoring contributions from the parasitic collisions). Table 2 compiles beam-beam tune shifts achieved at various colliders.

Table 2: Beam-beam tune shifts achieved at various hadron colliders and assumed in the LHC design, compared with those at two lepton colliders.

	ξ_{HO} / IP	no. of IPs	ξ total
SPS	0.005	3	0.015
Tevatron	0.01-0.02	2	0.02-0.04
RHIC	0.002	4	~0.008
LHC (design)	0.0034	2 (4)	~0.01
KEKB (e+e-)	0.07-0.11	1	0.07-0.11
LEP (e+e-)	0.08	4	0.32

It is interesting that the origin of the lower beam-beam tune shift at hadron colliders is not completely understood. For lepton colliders, such as KEKB, DAFNE and PEP-II, strong-strong simulations can accurately predict and reproduce achievable beam-beam tune shifts, in good agreement with quasi-strong or strong-strong simulations [47, 48]. However, applying the same codes to a hadron collider by turning off synchrotron radiation, and assuming an initially 'matched' beam distribution (a distribution whose shape remains unchanged in the course of the simulation), the simulated beam-beam tune shifts are much larger than those obtained with synchrotron radiation [47, 48], in stark contrast to the opposite experience at past and present hadron colliders. Possible explanations are that the actual hadron-beam distributions are not matched to the beam-beam interaction (and in the absence of synchrotron radiation may never assume the matched shape) or that for colliding hadron beams the beam-beam limit arises from additional noise, which is not yet properly included in these simulations. Reaching the same level of predictive power as established for leptons remains the ultimate goal of simulation efforts for hadron colliders like the LHC.

The long-range collisions contribute to the tune spread at large amplitude. Perhaps more importantly, they also give rise to a linear tune shift, which, unlike the head-on tune shift, is of opposite sign in the crossing plane and in the orthogonal direction. The long-range tune shift has the magnitude [9]

$$\xi_{LR} = 2n_{par}\frac{\xi_{HO}}{d^2}$$

where n_{par} denotes the total number of parasitic collisions (on either side of one IP) and d is the normalized beam-beam separation. For the LHC, with n_{par}=30, and d=9.5, we have ξ_{LR}~0.74 ξ_{HO}, i.e., the tune shift from the long-range collisions is comparable to the tune spread induced by the head-on collision.

The long-range tune shift would be inconsequential, if all bunches were identical. However, the two LHC beams consist of 39 trains of 72 bunches with 25-ns spacing arranged in a complicated pattern with gaps of various sizes, reflecting the rise times of various injection and extraction kickers in the injection chain and the LHC itself; see, e.g., [11]. As a result, different bunches encounter different numbers of long-range collisions and will, therefore, have different tunes. Most affected are the so-called 'PACMAN' bunches [9], i.e., the bunches at the start or end of a train, which experience the smallest number of long-range collisions. The effective tune spread over a bunch train can be markedly increased by the long-range effect, as is illustrated in Fig. 1. The long-range collisions appear to 'fold' the tune footprint. To minimize the

tune variation along the train, it is foreseen to cross the two beams at half of the IPs in the horizontal plane and at the other half in the vertical, which cancels the linear tune shifts from the long-range collisions between the IPs [9, 49].

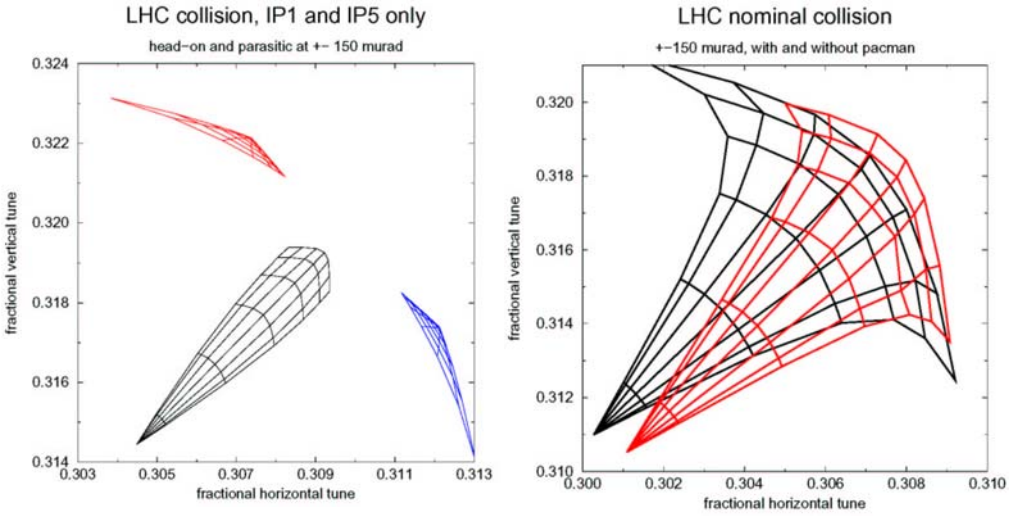

Figure 1: LHC tune footprints up to 6σ for the two high-luminosity IPs 1 & 5; the tune shift and spread from the head-on and long-range interaction of a nominal bunch (left); the total tune spread from the combined effect of head-on and long-range interaction for a nominal bunch and for a PACMAN bunch (right) [Courtesy H. Grote, 2001].

For the nominal LHC design parameters, the total tune spread in collision, from head-on beam-beam interaction, long-range collisions, and all other sources, does not exceed 0.015, a conservative value which was chosen based on the experience at the SPS collider and the Tevatron [1]. As indicated above, recent simulations by K. Ohmi [47, 48] suggest that, in principle, much higher tune shifts might be reached in hadron colliders, e.g., by proper shaping of the transverse beam distribution,

2.3.3 Dispersion & Crossing Angle

Synchro-betatron resonances reduce the permitted operating space in the tune diagram. These resonances are excited by the crossing angle, by dispersion at the collision point, and by dispersion at the rf cavities.

The Piwinski parameter, which characterizes the strength of a synchro-betatron sideband, for the crossing angle at IP 1 or 5 is

$$\phi_{piw,\theta} \equiv \frac{\sigma_z \theta}{\sigma^*_{x,y} 2} \approx 0.64 ,$$

comparable to the value at the KEK-B factory. The large Piwinski parameter from the crossing angle places the LHC in an interesting new regime for a hadron collider. However, the low synchrotron tune, about 0.002, will help avoiding the locations of harmful synchro-betatron resonances in the tune diagram.

There are two other side effects of the crossing angle, in addition to exciting synchro-betatron resonances. First, creating the crossing angle by orbit-corrector

magnets generates dispersion which, in the vertical plane, cannot be corrected. The maximum vertical dispersion in the arcs for a single IP with vertical crossing is about 0.3 m [50]. This corresponds to about D_y*=16 mm maximum vertical dispersion at IP 1 or 5, which also gives rise to synchro-betatron coupling. To compare the effect of this dispersion with the direct effect of the crossing angle we note that the resonance excitation from the crossing angle is equivalent to that generated by an IP dispersion of size $D^*_{y,\theta} \approx \theta\eta C/4\pi Q_s$, where η denotes the slippage factor, Q_s the synchrotron tune and C the circumference. For the LHC, this amounts to an equivalent IP dispersion of 100 mm, which is 6 times larger than the vertical IP dispersion created by the vertical crossing. Hence, the direct effect of the crossing angle dominates in the excitation of synchro-betatron coupling over the dispersive term. This can also be seen in the equivalent Piwinski parameter characterizing the effect of the dispersion due to the crossing angle at the IP, which amounts to only

$$\phi_{piw,D} \equiv \frac{D^*_y \sigma_\delta}{\sigma^*_y} \approx 0.11 ,$$

and, hence, is 6 times smaller than the Piwinski parameter for the crossing angle. However, in the LHC spurious dispersion resulting from misalignments, magnet-field errors, and orbit correction, can reach values up to several tens of cm at the IP [25, 51], in which case this spurious dispersion may become the major source of synchro-betatron coupling. The residual dispersion at the rf cavities yields another small contribution to synchro-betatron coupling, which, for the purpose of comparison, might be quantified by the equivalent Piwinski parameter

$$"\phi_{piw,rf}" \equiv \frac{k_{rf} e V_{rf}}{E_b} \frac{\sigma_z \sqrt{\beta H}}{\sigma_x} \frac{1}{4\pi\xi} \approx 0.1 ,$$

H being the dispersion invariant and β the beta function at the rf cavity.

Second, the crossing angle reduces the overlap of the two colliding beams, which decreases the luminosity. For the LHC, this geometric luminosity loss due to the crossing angle can be approximated as [43, 52]

$$\frac{L}{L_0} \approx \frac{1}{\sqrt{1+\phi^2_{piw,\theta}}} \approx 0.84 ,$$

which is significant. Luckily, the beam-beam tune shift is decreased by a similar reduction factor. For this reason, at the beam-beam limit colliding longer and more intense bunches with a larger crossing angle can increase the luminosity [43].

2.3.4 Loss of Landau Damping in the Strong-Strong Regime

If two proton beams collide, coherent oscillations are possible in the form of the so-called σ and π modes, where the bunches of either beam oscillate in phase or our of phase with respect to each other. For round beams, the frequency of the π mode is shifted by an amount 1.21ξ from the original tune. The factor 1.21 is called the Yokoya factor or Meller-Siemann-Yokoya factor after [31, 53]. Since this shift is larger than the total incoherent tune spread induced by the beam-beam interaction, ξ, the coherent π mode is not Landau damped and it may become unstable [32, 37]. The loss of Landau damping is predicted to occur, when the intensity of the weaker beam exceeds 60% of the intensity of the stronger beam [32, 37]. With equally strong beams

in the LHC, this is always the case, different from the situation in previous proton-antiproton colliders.

The Landau damping can be restored, by introducing an asymmetry between the two beams, for example, a tune difference of the order of ξ [33, 54]. The analytical predictions are based on a perturbative solution to the Vlasov equation [31, 32, 37]. They have been confirmed by multi-particle tracking studies [34, 35, 38, 36, 39], some of which also include the contribution from the long-range collisions. Broken symmetry for multiple interaction regions [39] may help to suppress the coherent π mode. However, in simulations, the excitation of higher-order coherent resonances is extremely sensitive to the local phase advance between two IPs, at the level of 0.02 ($x2\pi$), which will be difficult to control in practice [39]. The overlap with synchrotron sidebands weakens the coherent π mode too, though without its full suppression [40]. Unavoidable variations in intensity and beam sizes from bunch to bunch will have an additional remedial effect.

The only hadron collider presently operating in the strong-strong regime, RHIC, has occasionally observed the π mode in the Schottky tune spectrum, when tuning for lifetime [55]. For example, in RHIC the π mode was observed in operation with 55 bunches, colliding at 4 IPs. The measured tune distance between the π mode and the σ mode of 0.007 was consistent with the expected value of $1.21x4x\xi$, for ξ~0.0015. A tune change of 0.002 suppressed the π mode in RHIC. There was no observation of any beam instability. The RHIC results indicate that indeed, over most of the time, coherent beam-beam modes are suppressed by Landau damping due to naturally occurring asymmetries. The main limitation arising from coherent beam-beam modes at RHIC is a restriction of the tune space available for operation [55]. A similar situation may be expected for the LHC.

2.3.5 Diffusive Aperture due to Parasitic Collisions

Around each of the 4 main collision points, the two LHC beam experience 30 parasitic or long-range collisions. Table 3 illustrates that this number is much larger than at the SPS collider and still represents a significant increase with respect to the Tevatron Run-II, where the effect of long-range collisions has proven one of the key factors presently limiting performance [56].

Table 3: Number of long-range collisions at various hadron colliders

	No. of long-range encounters
SPS	9
Tevatron Run-II	70
LHC	120

The long-range collisions perturb the betatron motion at large amplitudes where particles come close to the opposing beam, and give rise to a so-called diffusive aperture d_a, which can result in enhanced background for the experiments and in a poor beam lifetime. An approximate scaling law for the magnitude of the diffusive aperture [2,7, 57] is

$$\left(d_{sep} - d_a\right)\Big/\sigma \propto \sqrt{k_{par} N_b / \varepsilon_N}$$

where $d_{sep}/\sigma \cong \theta_c/\sigma_\theta$ denotes the relative beam separation in units of the rms beam size σ, k_{par} is the total number of parasitic collisions around the two high-luminosity IPs, and σ_θ is the rms angular divergence at the IP. For the nominal LHC beam emittance and separation schemes with k_{par}=2x30 parasitic encounters, simulation results [7] suggest that this scaling law can be written [57]

$$\frac{d_{da}}{\sigma} \approx \theta_c \sqrt{\frac{\beta^*}{\varepsilon_n}} - 3\sqrt{\frac{N_b}{10^{11}}}$$

in qualitative agreement with particle-tracking results for the dynamic aperture of a complete LHC model [6, 58]. For nominal parameters, the normalized beam separation is about 9.5σ and the diffusive aperture 6.0-6.5σ. In other words, the long-range collisions reduce the dynamic aperture by about 3σ from the value estimated purely from the ratio of crossing angle and IP beam divergence.

For low beam intensities the effect of the long-range collisions is diminished and the diffusive aperture may even disappear. Figure 2 compares simulated diffusion rates for the nominal LHC beam with those for two different commissioning beams [59]. Neither commissioning beam experiences a sharp diffusive aperture as seen for the nominal parameters. The case of larger bunch spacing (scenario 1) is particularly benign.

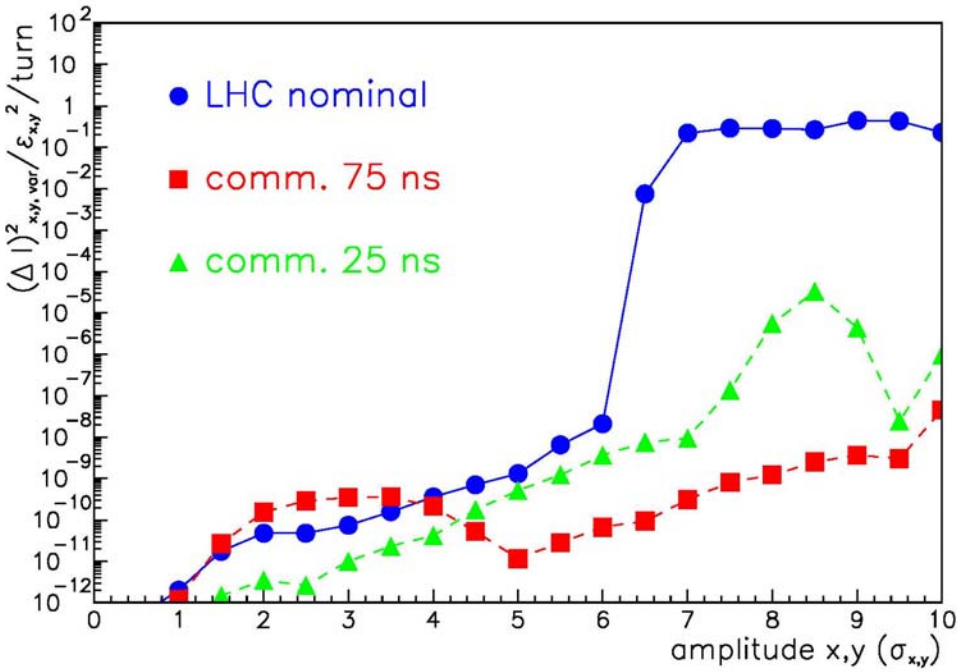

Figure 2: Simulated action diffusion rate (in units of the squared nominal emittance per turn) as a function of amplitude for LHC with two IPs and alternating crossing for the nominal LHC beam and for two commissioning beams with reduced intensity and relaxed parameters (scenario 1: 75-ns spacing, β^*=1.0 m, ε_n= 3.75 μm, N_b=9x10^{10}, θ_c=250 μrad; scenario 2: 25-ns spacing, β^*=0.55 m, ε_n= 3.75 μm, N_b=4x10^{10}, θ_c=285 μrad).

2.3.6 Choice of Crossing Scheme

The planned installation of beam screens – with either vertical or horizontal orientation - inside the final-triplet quadrupoles, for vacuum reasons, requires a decision on the crossing scheme. In the present baseline design, it is foreseen to cross the two beams in one high-luminosity IP horizontally and in the second vertically. This minimizes the tune variation between bunches [9, 13], and, to a lesser extent, also the variation in orbit offsets and chromaticity [13].

Known disadvantages of alternating collisions are the introduction of vertical dispersion, which cannot be corrected, and breaking the symmetry between the two high-luminosity experiments, which, unlikely but possibly, could result in different running conditions [13].

In addition, weak-strong beam-beam simulations with the code WSDIFF consistently show that the diffusive aperture tends to be larger with horizontal-horizontal or vertical-vertical crossing, as compared with horizontal-vertical crossing [14]. Example results of these simulations are shown in Fig. 3.

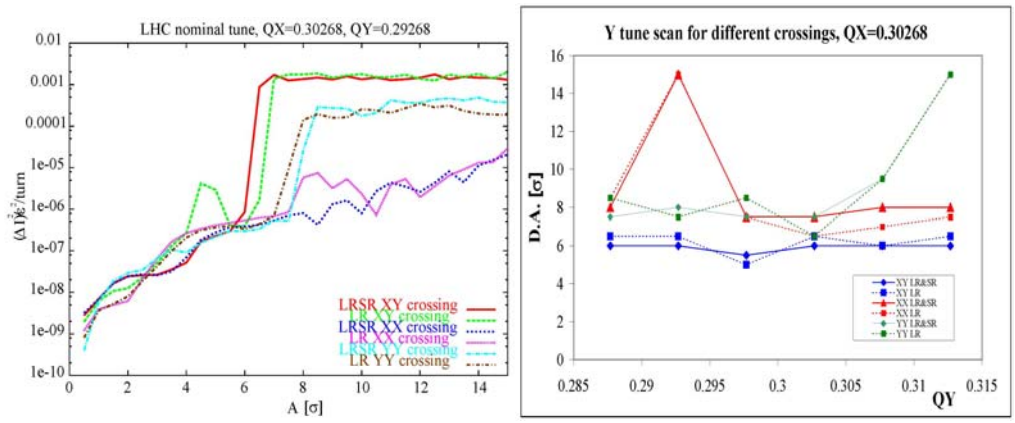

Figure 3: Simulated diffusion rate as a function of start amplitude for XX, XY and YY crossing with LR only and with the combined effect of LR and SR collisions, for the same 0-amplitude tunes QX=0.30268, QY=0.29268 (left); and the diffusive aperture for the different crossing schemes, inferred from simulations like that on the left, as a function of the vertical tune (right).

The reason for the increased stability in the case of equal-plane crossing is not fully understood. The diffusive aperture caused by long-range collisions has been estimated analytically in 1-D using Chirikov's overlap criterion [8], and in 2-D by the location of folds in the frequency map [60]. Unfortunately, neither of these approaches seems to explain the observed dependence on the crossing scheme. Instead we can imagine the following two aspects to matter. In the case of equal-plane crossing about half as many resonances are excited as for alternating crossing, thus reducing the likelihood of 2-D resonance overlap. Also, alternating crossing does not only cancel the base tune shift, but also the tune shift quadratic in action, whereas the linear tune shift with action is independent of the crossing scheme. It may be that the higher-order detuning terms which are removed by the alternating crossing have a stabilizing effect.

2.3.7 Beam-Beam Compensation

In the past, numerous attempts were made to compensate the linear and nonlinear forces of the beam-beam interaction in order to overcome the beam-beam limit. Famous are the 4-beam collisions at DCI [61, 62]. The charge neutralization between electron and positron beams was supposed to cancel all net forces and to allow for high luminosity. Unfortunately, collective instabilities limited the DCI performance. At the CERN ISR a nonlinear lens was in operation from 1975, which modeled the effect of a 'head-on' collision [63]. The nonlinear lens was formed by two copper bars fed with 1000 A current. The experiments showed that resonances of order 10 or higher contribute to the proton beam-beam limit. The possibility of compensating the beam-beam tune spread using octupoles was explored in simulations for LEP [64] and experimentally at VEPP-4/-2M [65, 66] and DAFNE [67]. Also, a plasma-based compensation was proposed for linear electron-positron [68] as well as for muon colliders [69]. Compensation of beam-beam effects in hadron colliders by a low-energy electron beam was proposed for the SSC [70]. Since 2001, the Tevatron Electron Lens (TEL) [71] is operational at FNAL. In the near future, a pair of TELs will be capable of compensating both the intra- and inter-bunch tune spread in the Tevatron antiproton beam [71, 72].

To correct the nonlinear effects of the long-range collisions in the LHC, a correction scheme was proposed [15, 16], which consists of a wire running parallel to the beam approximately the same transverse distance in units of rms beam size as the opposing beam at the parasitic collision points. The wire is mounted where the beams are already separated, but the betatron phase still is approximately the same as at the points of the long-range encounters. The proposed location of the long-range compensators in the LHC is 41m downstream of the separation dipoles D2 on both sides of IP1 and IP5, as sketched in Fig. 4. The average difference in betatron phase between the compensator and the associated long-range collisions is 2.6^{o} [15], which, according to simulations, is sufficiently close to zero [17].

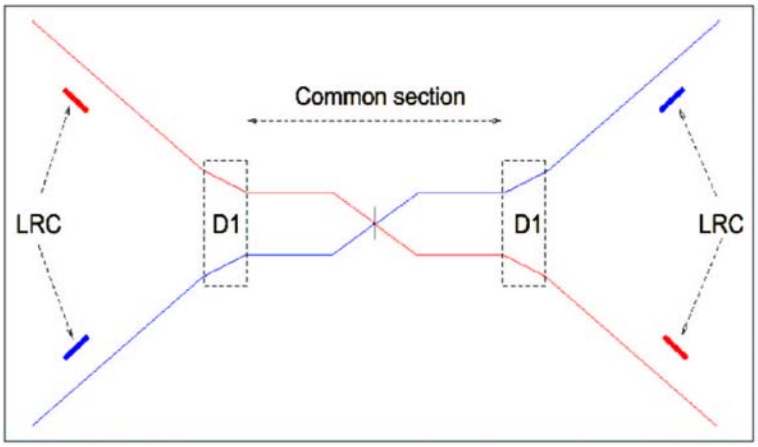

Figure 4: Schematic of the LHC long-range beam-beam compensators (LRCs) mounted on either side of IP1 and IP5 upstream of the separation dipoles [15, 16].

2.3.8 Beam Experiments at the SPS

Several prototype beam-beam compensators have been built and installed in the SPS. These allow us to experimentally model the effect of LHC long-range collisions and, using two wires at different locations, to study their compensation and the related tolerances. In addition, with various wires mounted in the vertical plane, in the horizontal plane, and at 45 degree, we can investigate the efficiency of different crossing schemes. Figure 5 compares simulated diffusion rates due to long-range collisions in the LHC and due to a single wire in the SPS. The effect is quite similar. Figure 6 shows one of the prototype devices installed in the SPS.

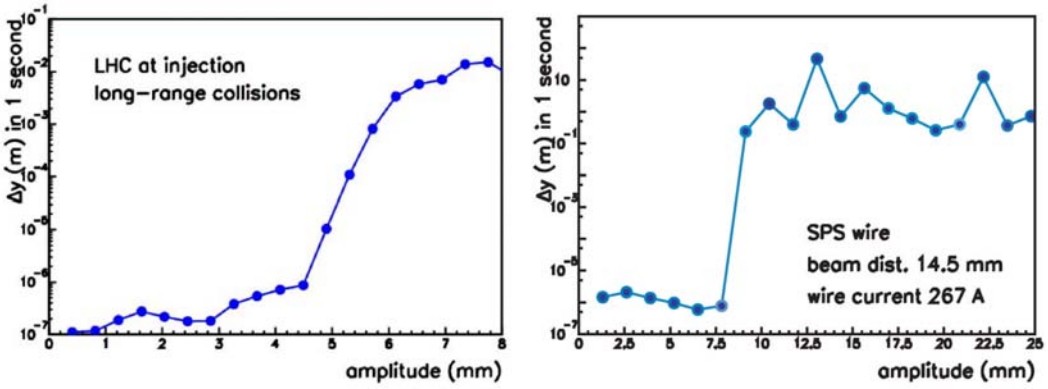

Figure 5: Simulated amplitude growth in mm during 1 second due to long-range beam-beam collisions in the LHC at injection (left) and die to the wire at 267-A excitation in the SPS at 55 GeV/c (right) as a function of starting amplitude, for β=80 m (LHC) or 50 m (SPS).

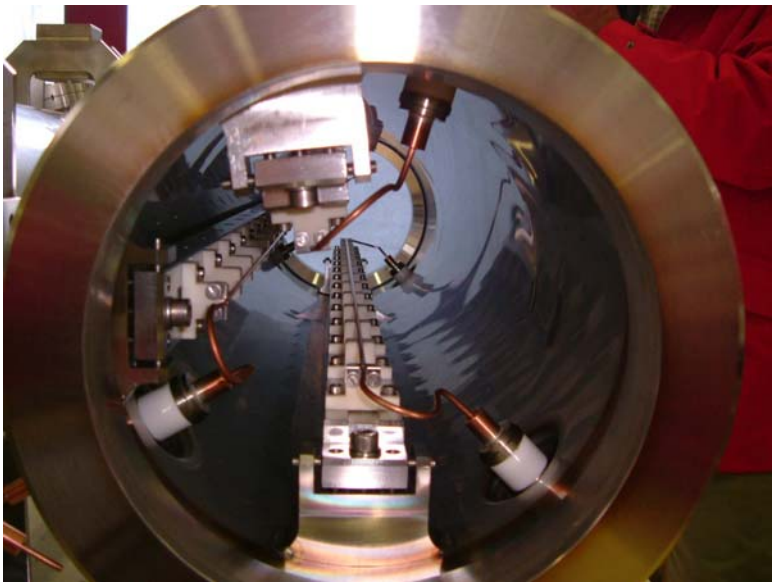

Figure 6: Photo of a new 3-wire long-range beam-beam compensator installed at the SPS in 2004.

The SPS beam experiments started in 2002. Measured changes in orbit and tune induced by the wire are consistent with predictions and allow for an exact calibration of the beam-wire distance. Various additional signals provide information on the nonlinear effect of the wire: loss signals and lifetime, final emittance of an initially blown-up beam, loss-signal response to scraper retraction, and multi-turn beam-position data after kicking a 'pencil beam'. The experiments with a single wire are discussed in [19, 20]. The result of a first attempt at compensation is displayed in Fig. 7. The beam lifetime drops significantly, if a single wire is excited, representing the effect of LHC long-range collisions. Activating a second wire at optimum setting, modeling the LHC compensation, almost restores the original lifetime for most values of the vertical tune. Why the lifetime is not fully recovered for Q_v below 0.29 is not yet understood; this apparent imperfect correction might reflect a drift in some uncontrolled parameter during the experiment or have a more complex origin.

Latest news on long-range beam-beam compensation in SPS and LHC can be found at the web site: *http://cern-ab-bblr.web.cern.ch/cern-ab-bblr/* .

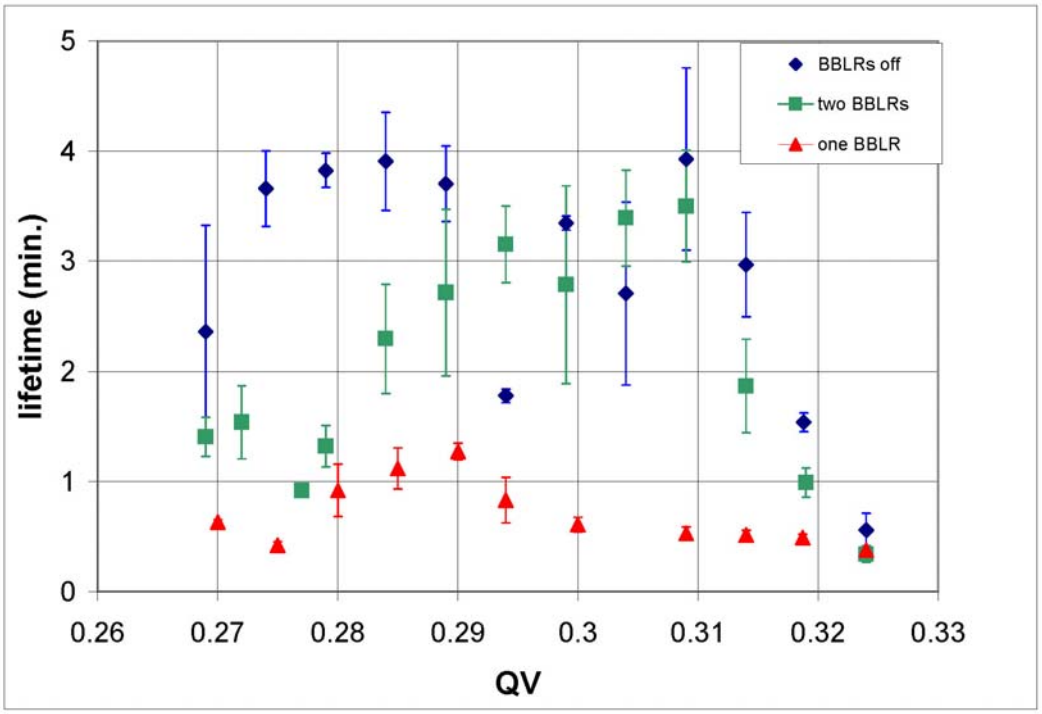

Figure 7: Beam lifetime in the SPS without wire, with a single wire, and with two compensating wires as a function of the vertical tune, for a horizontal tune of 0.31, and a wire excitation of 240 A (the effective wire length is 1.2 m); the beam lifetime was inferred from the intensity loss during the time period of wire excitation (about 2.4 s) [73].

2.3.9 Luminosity Optimization for LHC Upgrade

The LHC experiments have expressed interest in an upgrade for higher luminosity. An upgrade feasibility study was conducted from 2000 to 2001 [57]. There are two different paths to upgrade the LHC and to increase its luminosity. Both paths envision

a reduction of the IP beta function by a factor of 2 and an associated increase in the crossing angle by a factor of $\sqrt{2}$. One approach installs additional higher-harmonic rf to shorten the bunches and to recover the original geometric luminosity reduction factor. The second approach assumes that the single bunch population can be increased above the ultimate bunch intensity so as to reach the beam-beam limited tune shift for the larger crossing angle and longer bunches. An additional factor of $\sqrt{2}$ is gained if the longitudinal bunch profile is chosen uniform instead of Gaussian (such uniform or 'hollow' bunches can be created either already in the CERN PS [74] or in the LHC at top energy [75]). The total circulating beam current is confined by reducing the number of bunches, which also suppresses any electron cloud activity. An extreme case of this approach is to store a single superbunch. The different options are summarized in Table 4. None of these options includes the use of crab cavities, which are discussed further below. Crab cavities would relax the requirements of the first upgrade path and allow for 20% higher luminosity.

Table 4: List of LHC parameters at 7 TeV corresponding to different luminosity upgrade scenarios

parameter	**symbol**	**shorter bunches**	**longer bunches**	**superbunch**
#bunches	n_b	5616	936	1
protons/bunch	N_b [10^{11}]	1.7	6.0	5600
bunch spacing	Δt_{sep} [ns]	25	75	89000
average current	I [A]	0.86	1.0	1.0
norm. trans. emittance	ε_n [μm]	3.75	3.75	3.75
longit. profile		Gaussian	uniform	uniform
rms bunch length	σ_z [cm]	3.78	14.4	6000
beta at IP1 & IP5	β^* [m]	0.25	0.25	0.25
full crossing angle	θ_c [μrad]	445	430	1000
Piwinski parameter	$\theta_c \sigma_z / (\sigma^* 2)$	0.75	2.8	2700
luminosity	L [10^{34} cm^{-2}s^{-1}]	4.6	8.9	9.0
events/ crossing		88	510	5×10^5
length luminous region (rms)	σ_{lum} [mm]	21.8	36.3	16.7

The second upgrade path is based on an analytical calculation of the luminosity and the total tune shift for a collider with two IPs and alternating crossing [43, 44]. For a small crossing angle, $\theta_c << 1$, a full crossing angle larger than the rms beam divergence, i.e., $\theta_c >> \sqrt{\varepsilon / \beta^*}$, and a total bunch length l_{flat} larger than the effective length of the interaction region, or $l_{flat} > 10\sigma^* / \theta_c$, the total tune shift for uniform bunches, reduces to

$$\Delta Q_{tot} \approx -\sqrt{\frac{2}{\pi}} \frac{r_p \beta^*}{\gamma \sigma^* \theta_c} \lambda$$

and the luminosity to

$$L \approx \frac{f_{coll} l_{flat} \lambda^2}{\sqrt{\pi}} \frac{1}{\theta_c \sigma^*}.$$

where λ denotes the (constant) bunch line density and $f_{\rm coll}$ the collision frequency. Combining the last two equations yields

$$L \approx \frac{f_{coll} \gamma \varepsilon_n}{r_p{}^2 \beta^*} \Delta Q_{tot}^2 \frac{\sqrt{\pi} \theta_c l_{\rm flat}}{2\sigma^*}$$

which is proportional to the crossing angle θ_c and to the total length of the super-bunch $l_{\rm flat}$. We can also express the luminosities in terms of the total tune shift and the total bunch population N_b as

$$L \approx \frac{1}{\sqrt{2}} \frac{f_{coll} \gamma}{r_p \beta^*} \Delta Q_{tot} N_b$$

For a Gaussian profile the expression for the total tune shift remains the same, if we simply replace λ by the peak line density, and the luminosity is given by the last expression divided by an additional factor of $\sqrt{2}$. Figure 8 shows the possible luminosity gain in the LHC that can be achieved by increasing the Piwinski angle with bunches of either Gaussian or uniform profile. Here, the beam-beam limit is taken to correspond to a total tune shift of 0.01 from two IPs. The curves assume that the bunch population is increased together with the bunch length or the crossing angle, so as to maintain a constant tune shift of 0.01.

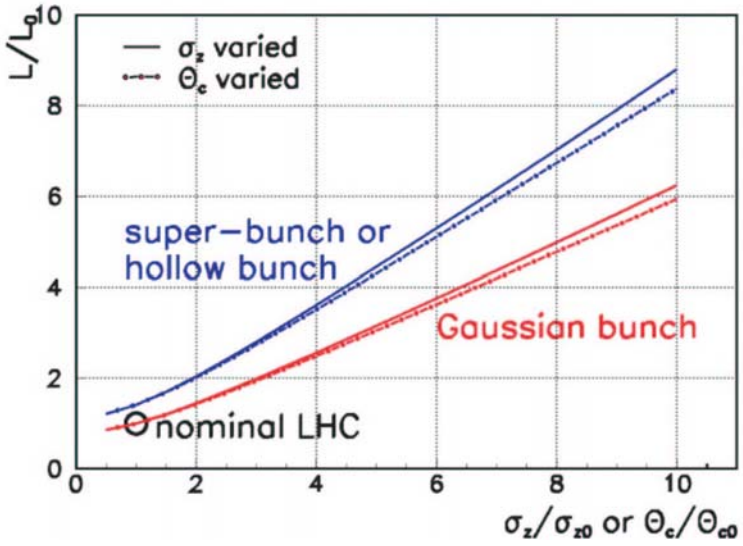

Figure 8: Relative luminosity gain for the Large Hadron Collider as a function of the relative increase in crossing angle or bunch length for a uniform bunch profile or super-bunches (top curves) and for regular Gaussian bunches (bottom curves). The vertical axis is normalized to a base luminosity at the beam-beam limit with two IPs of L_0=2.3x10^{34} cm^{-2}s^{-1} and the horizontal axis to an rms bunch length of σ_{z0}=7.6 cm or to a crossing angle θ_0=300 μrad [43, 44].

For completeness, we note that the rms length of the luminous region in Table 4 is obtained from

$$\frac{1}{\sigma_{lum}^2} \approx \left(\frac{2}{\sigma_s^2} + \frac{\theta_c^2}{2\sigma_x^{*2}} \right).$$

2.3.10 Ground Motion

Ground motion leads to transverse displacements of the quadrupole magnets, which in turn deflect the orbit. Unlike for electron-positron or proton-antiproton colliders, in sections with a single beam pipe and common magnets, at the LHC the deflection from a displaced quadrupole has opposite sign for the two counter-propagating proton beams of the LHC. Therefore, the ground motion will separate the beams at the collision points. To consider a worst-case scenario, we may assume a random beam-beam offset, Δx, varying from turn to turn. For n_{IP} IPs, this random offset generates the emittance growth [14]

$$\frac{\Delta\varepsilon}{\Delta t} \approx n_{IP} 8\pi^2 \left(\Delta x\right)_{rms}^2 \xi_{HO}^2 f_{rev} \frac{1}{\beta^*},$$

where we computed the emittance increase from uncorrelated dipole kicks for a linear beam-beam force. Demanding less than 10% emittance growth per hour for a SuperLHC with β^*=0.25 m, n_{IP}=2, ξ_{HO}=0.005, γ~7000 and $\gamma\varepsilon$=3.75 μm, the tolerances on the turn-to-turn variation is Δx<8 nm, less than 0.1% of the rms spot size. The 8-nm tolerance on the beam-beam separation approaches values familiar from linear colliders. What helps in case of the LHC is the high revolution frequency of about 11 kHz, where, e.g., ground motion amplitudes are small.

Considering a working point far from low-order resonances, and taking into account the measured ground motion spectrum [76] as well as the response of the lattice [21], a much more detailed and accurate analysis of the emittance growth due to the measured correlated ground motion was performed by T. Sen and M.-P. Zorzano [23] following the procedure of [77]. They found that natural ground motion together with the head-on beam-beam interaction would double the LHC emittance only after 1000 days, i.e., that ground motion is a negligible effect.

2.3.11 Crab cavities

To combine all the advantages of a crossing angle with those of a head-on collision, crab cavities were proposed first for linear colliders [45] and soon after for storage rings [46]. The crab cavity is an rf cavity operating in a transverse dipole mode, whose phase with respect to the beam is adjusted such that the head and tail of a bunch are deflected in opposite directions and the center of the bunch unaffected, and in the centre-of-mass frame the collision becomes head on. Since there is neither geometric luminosity reduction nor excitation of synchro-betatron resonances, the crab crossing scheme would allow for large crossing angles and, thereby, avoid the problem of the long-range collisions. In 2005 for the first time a crab cavity will be installed at an operating collider, KEKB. Table 5 compares the parameters of the KEKB crab cavity with example parameters for an LHC upgrade with an 8 mrad crossing angle, sufficiently large to accommodate two separate final quadrupoles for the two beams [78] and well above the values considered for other LHC upgrade paths, e.g., in [57].

For a 90-degree betatron phase advance between the crab cavity and the collision point, the crab cavity voltage required is

$$V_{crab} = \frac{cE_b \tan(\theta_c / 2)}{e\omega_{rf}\sqrt{\beta^* \beta_{crab}}}.$$

If the rf phases of the crab cavities on either side of the collision point drift with respect to each other, a net deflection of the beam center results that will lead to an off-center collision and emittance growth. If Δx denotes the acceptable change in transverse position offset the associated tolerance on the relative crab-cavity rf phase stability is

$$\Delta\phi \le 2\pi \frac{\Delta x}{\lambda_{rf}\theta_c}.$$

Crab cavities for higher beam currents, up to 10 A, are under development [79]. For a hadron collider like LHC or SuperLHC, the RF noise in the crab cavities could be a significant source of emittance growth, and, therefore, it may need to be limited to levels much lower than what is acceptable in lepton colliders. Alternatively, the effect of crab-cavity phase noise could be corrected by a transverse feedback system.

Table 5: Crab-cavity parameters for KEKB [80] and an example parameter set for a SuperLHC [14]

variable	symbol	KEKB HER	SuperLHC
beam energy	E_b	8 GeV	7 TeV
rf frequency	f_{crab}	508.9 MHz	1.3 GHz
full crossing angle	θ_c	22 mrad	8 mrad
IP beta function	β^*	0.33 m	0.25 m
crab-cavity beta function	β_{cav}	100 m	2 km
kick voltage	V_{crab}	1.44 MV	46 MV
phase tolerance	$\Delta\phi_{crab}$	not specified	0.06 mrad

2.3.12 Summary

The LHC is expected to experience a number of exciting and novel beam-beam phenomena, such as the dominant effect of long-range collisions, the sensitivity to relative orbit motion at the 10-nm level, and the possible loss of Landau damping in the strong-strong regime. To overcome any beam-beam limitations encountered at the baseline LHC, future upgrades to the LHC will likely employ some advanced techniques, such as wire-based long-range beam-beam compensation, crab cavities, active stabilization, and operation with long bunches or 'superbunches' at increased crossing angles. Although lots of LHC beam-beam studies have been performed in the past, uncertainties still remain. For example, it is not yet possible to predict the maximum achievable beam-beam tune shift of hadron colliders by computer simulations. Preliminary results from strong-strong or quasi-strong simulations indicate that proper beam shaping may be essential for reaching higher tune shifts with hadron beams. The effect of noise and related tolerances are under exploration. The beam-beam effect could be enhanced by an electron cloud [81, 82]. Another open question concerns the optimum choice of the crossing plane at the various IPs, and in particular the underlying reason why the particle dynamics for alternating crossing appears less stable than for equal-plane crossing. An experimental simulation of the

LHC long-range beam-beam collisions and their compensation is underway at the CERN SPS.

2.3.13 Epilogue

The LHC beam-beam studies greatly benefit from the experience gained at previous hadron and lepton collliders, as well as from the copious pioneering studies which were performed for the SSC.

More details of the various topics can be found in the references quoted. In particular, many results of beam-beam studies for the LHC and other hadron colliders were presented and discussed at the workshops on 'Beam-Beam Effects in Large Hadron Colliders,' LHC99 [83], on 'Beam-Beam Effects in Circular Colliders' [84], and on 'Beam-Beam Effects in Ring Colliders' [55].

Multi-laboratory joint beam-beam studies for LHC, Tevatron and RHIC have recently been reinforced, e.g., in the framework of the European CARE and the US LARP programs; see the web sites *http://care-hhh.web.cern.ch/CARE-HHH/* and *http://www.agsrhichome.bnl.gov/LARP/*. There is no lack of interesting and challenging problems.

2.3.14 References

1. O. Bruning, et al., 'LHC Design Report. Volume I – The LHC Main Ring,' CERN-2004-003 (2004).
2. J. Irwin, "Diffusive Losses from SSC Particle Bunches Due to Long-Range Beam-Beam Interactions," SSC-233 (1989).
3. W. Chou, D. Ritson, "Dynamic Aperture Studies During Collisions in the LHC," LHC Project Report 123 (1997).
4. J. Miles, M. Boege, "Overview of the LHC Dynamic Aperture Studies," LHC Project Report 106 (1997).
5. T. Sen et al., "Effect of the Beam-Beam Interaction on the Dynamic Aperture and Amplitude Growth in the LHC," Proc. 'Beam-Beam Effects in Large Hadron Colliders' (LHC99), CERN, Geneva, eds. J. Poole, F. Zimmermann, CERN-SL-99-039-AP (1999).
6. H. Grote, F. Schmidt, L.H.A. Leunissen, "LHC Dynamic Aperture in Collision," CERN LHC Project Note 197 (1999).
7. Y. Papaphilippou, F. Zimmermann, "Weak-Strong Beam-Beam Simulatons for the LHC," Proc. 'Beam-Beam Effects in Large Hadron Colliders' (LHC99), CERN, Geneva, eds. J. Poole, F. Zimmermann, CERN-SL-99-039-AP (1999); and Phys. Rev. Special Topics – Accel. Beams 2, 104001 (1999).
8. Y. Papaphilippou, F. Zimmermann, "Estimates of Diffusion due to Long-Range Beam-Beam Collisions," Phys. Rev. Special Topics – Accel. Beams 5, 074001 (2002).
9. D. Neuffer, S. Peggs, "Beam-Beam Tune Shifts and Spreads in the SSC: Headon, Long Range and PACMAN Conditions," SSC-63 (1986).
10. W. Herr, "Effects of PACMAN Bunches in the LHC," CERN LHC Project Report 39 (1996).

11. J. Jowett, "Filling Schemes, Collision Schedules, and Beam-Beam Equivalence Classes," Proc. 'Beam-Beam Effects in Large Hadron Colliders' (LHC99), CERN, Geneva, eds. J. Poole, F. Zimmermann, CERN-SL-99-039-AP (1999).
12 .H. Grote, W. Herr, "Self-Consistent Orbits with Beam-Beam Effects in the LHC," in CERN LHC Project Report 502 (2001) and Proc. Workshop on 'Beam-Beam Effects in Circular Colliders', Fermilab, Batavia, June 2001, eds. T. Sen, M. Xiao, FERMILAB-CONF-01-390 (2002).
13. W. Herr, "Features and Implications of Different LHC Crossing Schemes," CERN LHC Project Report 628 (2003).
14. F. Zimmermann, "Beam Dynamics Challenges for Future Circular Colliders," EPAC04 Lucerne (2004).
15. J.-P. Koutchouk, "Principle of a Correction of the Long-Range Beam-Beam Effect in LHC Using Electromagnetic Lenses," LHC Project Note 223 (2000).
16 .J.-P. Koutchouk, "Correction of the Long-Range Beam-Beam Effect in LHC Using Electro-Magnetic Lenses," PAC01 Chicago, and CERN-SL-2001-048-BI (2001).
17 .F. Zimmermann, "Weak-Strong Simulation Studies for the LHC Long-Range Beam-Beam Compensation," presented at Workshop on 'Beam-Beam Effects in Circular Colliders', Fermilab, Batavia, June 2001, eds. T. Sen, M. Xiao, FERMILAB-CONF-01-390 (2002).
18. L. Jin, J. Shi, W. Herr, "Study of the Wire Compensation of Long-Range Beam-Beam Interactions in LHC with a Strong-Strong Beam-Beam Simulation," EPAC 2002 Paris (2002).
19. J.-P. Koutchouk, J. Wenninger, F. Zimmermann, "Compensating Parasitic Collisions using Electromagnetic Lenses," Proc. Factories'03 Stanford, and CERN-AB-2004-011 (ABP).
20 .J.-P. Koutchouk, J. Wenninger, F. Zimmermann, "Experiments on LHC Long-Range Beam-Beam Compensation in the SPS," EPAC04 Lucerne (2004).
21 .E. Keil, "Effect of Plane Ground Waves on the Closed Orbit in Circular Colliders," CERN-SL-97-061-AP (1997).
22. L. Vos, "Effect of Very Low Frequency Ground Motion on the LHC," Proc. 'Beam-Beam Effects in Large Hadron Colliders' (LHC99), CERN, Geneva, eds. J. Poole, F. Zimmermann, CERN-SL-99-039-AP (1999).
23. M.-P. Zorzano, T. Sen, "Emittance Growth of the LHC Beam due to the Effect of Head-On Beam-Beam Interaction and Ground Motion," EPAC2000 Vienna (2000).
24. A. Verdier, L. Vos, "Ground Motion Model for the LHC," LHC Project Report 444 (2000).
25. L.H.A. Leunissen, "Influence of Vertical Dispersion and Crossing Angle on the Performance of the LHC," Proc. 'Beam-Beam Effects in Large Hadron Colliders' (LHC99), CERN, Geneva, eds. J. Poole, F. Zimmermann, CERN-SL-99-039-AP (1999).
26. R. Assmann, F. Schmidt, F. Zimmermann, M.-P. Zorzano, "Equilibrium Distribution and Halo in the LHC," EPAC 2002, Paris (2002).
27. S. Krishnagopal, M.A. Furman, W.C. Turner, "Studies of the Beam-Beam Interaction for the LHC," PAC99 New York (1999).
28. J. Shi, D. Yao, "Collective Beam-Beam Effects in Hadron Colliders," Phys. Rev. E 62, 1258 (2000).
29. M.A. Furman, W.C. Turner, "Beam-Beam Simulations for Separated Beams in the LHC," EPAC2000 Vienna (2000).

30. B. Muratori, "Study of Offset Collisions and Beam Adjustment in the LHC Using a Strong-Strong Simulation Model," EPAC2002 (2002).
31. K. Yokoya, Y. Funakoshi, E. Kikutani, H. Koiso, J. Urakawa, "Tune Shift of Coherent Beam-Beam Oscillations," KEK Preprint 89-14 and Part. Acc. 27, 181 (1990).
32. Y. Alexahin, "On the Landau Damping and Decoherence of Transverse Dipole Oscillatons in Colliding Beams," Part. Acc. 59, 43 (1996).
33. A. Hofmann, "Beam-Beam Modes for Two Beams with Unequal Tunes," Proc. 'Beam-Beam Effects in Large Hadron Colliders' (LHC99), CERN, Geneva, eds. J. Poole, F. Zimmermann, CERN-SL-99-039-AP (1999).
34. M.-P. Zorzano, F. Zimmermann, "Coherent Beam-Beam Oscillations at the LHC," CERN LHC Project Report 314 and Phys. Rev. Special Topics – Accel. Beams 3, 044401 (2000).
35. W. Herr, M.-P. Zorzano, F. Jones, "A Hybrid Fast Multipole Method Applied to Beam-Beam Collisions in the Strong-Strong Regime," Phys, Rev. Special Topics – Accel. Beams 4, 054402 (2001).
36. Y. Alexahin, H. Grote, W. Herr, M.-P. Zorzano, "Coherent Beam-Beam Effects in the LHC," CERN LHC Project Report 466 (2001).
37. Y. Alexahin, "A Study of the Coherent Beam-Beam Effect in the Framework of the Vlasov Perturbation Theory," Nucl. Inst Meth. A 380, 253 (2002).
38. Y. Alexahin, M.-P. Zorzano, "Excitation of Coherent Beam-Beam Resonances for Beams with Unequal Tunes in the LHC," CERN LHC Project Note 226 (2000).
39. W. Herr and M.-P. Zorzano, "Coherent Dipole Modes for Multiple Interaction Regions," CERN LHC Project Report 461 (2001).
40. W. Herr and R. Paparella, "Landau Damping of Coherent Dipole Modes by Overlap with Synchrotron Sidebands," CERN LHC Project Note 304 (2002).
41. F.W. Jones, W. Herr, "Parallel Computation of Beam-Beam Interactions Including Longitudinal Motion," PAC2003 Portland (2003).
42. L. Jin, J. Shi, "Importance of Beam-Beam Tune Spread to Collective Beam-Beam Instability in Hadron Colliders," Phys. Rev. E69, 036503 (2004).
43. F. Ruggiero, F. Zimmermann, "Luminosity Optimization Near the Beam-Beam Limit by Increasing Bunch Length or Crossing Angle," PRST-AB 5, 061001 (2002).
44. F. Ruggiero, F. Zimmermann, G. Rumolo, Y. Papaphilippou, "Beam-Beam Interaction, Electron Cloud, and Intrabeam Scattering for Proton Superbunches," PAC03 Portland (2003).
45. R.B. Palmer, "Energy Scaling, Crab Crossing and the Pair Problem," DPF Summer Study Snowmass '88: 'High Energy Physics in the 1990's', Snowmass, Colorado (1988).
46. K. Oide, K. Yokoya, "The Crab Crossing Scheme for Storage Ring Colliders," Phys. Rev. A40, 315 (1989).
47. K. Ohmi, M. Tawada, K. Oide, "Study of the Mechanism of the Beam-Beam Limit," Proc. Factories'03, Stanford, ed. J. Seeman (2003).
48. K. Ohmi, M. Tawada, K. Oide, D. Kamada, "Study of the Diffusion Processes Caused by the Beam-Beam Interactions," APAC 2004, Gyeongju, Korea (2004).
49. W. Herr, "Tune Shifts and Spreads due to Short-Range and Long-Range Beam-Beam Interactions in the LHC," CERN/SL/90-06 (AP) (1990).
50. F. Meot, "Correction of Vertical Crossing Induced Dispersion in LHC," LHC-Project-Note-122 (1997).

51. R. Assmann, S. Fartoukh, F. Zimmermann, "Measuring Beta Functions and Dispersion in the Early LHC," EPAC 2002 Paris (2002).
52. B. Muratori, "Luminosity in the Presence of Offsets and a Crossing Angle," CERN AB-Note-2003-026 (ABP).
53. R.E. Meller, R.H. Siemann, "Coherent Normal Modes of Colliding Beams," IEEE Trans. NS-28, p. 2431 (1981).
54. Y. Alexahin, "Eigenmodes of Coherent Oscillations in Colliding Beams," Proc. 'Beam-Beam Effects in Large Hadron Colliders' (LHC99), CERN, Geneva, eds. J. Poole, F. Zimmermann, CERN-SL-99-039-AP (1999).
55. W. Fischer, "Observation of Strong-Strong and Other Beam-Beam Effects in RHIC," Proc. Beam-Beam Workhop 2003, Montauk, in conjunction with HALO'03 Workshop, to be published.
56. T. Sen, "New Aspects of Beam-Beam Phenomena in Hadron Colliders", PAC2003 Portland Oregon (2003).
57. O. Bruning et al., "LHC Luminosity and Energy Upgrade: A Feasibility Study," LHC Project Report 626 (2002).
58. Y. Luo, F. Schmidt, "Weak-Strong Beam-Beam Tracking for LHC v6.1," CERN LHC Project Report 502, and Proc. Workshop on 'Beam-Beam Effects in Circular Colliders', Fermilab, Batavia, June 2001, eds. T. Sen, M. Xiao, FERMILAB-CONF-01-390 (2002).
59. F. Ruggiero, "Parameters for 1st Physics and for 10^{33}," Proc. LHC Performance Workshop Chamonix XII, CERN-AB-2003-008 ADM (2003).
60. J. Laskar, "Frequency Map Analysis and Particle Accelerators," Proc. PAC 2003 Portland Oregon, p. 378 (2003).
61. J. Le Duff et al., "Space Charge Compensation with DCI," Proc. 11th International Conference on High-Energy Accelerators, Geneva (1980).
62. Ya. S. Derbenev, "Collective Instability of Compensated Colliding Beams," SLAC-TRANS-0151 (1973) and IYF-70-72 (1972).
63. E. Keil, G. Leroy, "Effects of a Non-Linear Lens on the Stored Proton Beam in the ISR," CERN/ISR-TH-GE/75-18 and PAC 1975 Washington (1975).
64. S. Myers, "Increase of the Beam-Beam Limit by Compensation of the Beam-Beam Tune Dependence on Amplitude," CERN-LEP-Note-400 (1982).
65. A.B. Temnykh, "Influence of Cubic Nonlinearity of Storage Ring Magnetic Field on the Beam-Beam Effects on VEPP-4," Proc. of XIII International Conference on High-Energy Accelerators, Novosibirsk, v. 1, p. 78 (1986).
66. A.B. Temnykh, "Observation of Beam-Beam Effects on VEPP-4," Proc. 3rd Advanced ICFA Beam Dynamics Workshop on Beam-Beam Effects in Circular Colliders, Akademgorodok, Novosirbirsk, eds. I. Koop and G. Tumaikin (1989).
67. M. Zobov, "Crosstalk between Beam-Beam Effects and Lattice Nonlinearities in DAFNE," DAFNE Technical Note G-57 (2001).
68. D.H. Whittum, A.M. Sessler, J.J. Stewart, S.S. Yu, "Plasma Suppression of Beamstrahlung," Part. Acc. 34: 89-104 (1990).
69. K.V. Lotov, "Constraints of Plasma Compensation of Beam-Beam Effects in Muon Colliders," Phys. Rev. E 63, 036503 (2001).
70. E. Tsyganov, R. Meinke, W. Nexsen, A. Zinchenko, "Compensation of the Beam-Beam Effect in Proton-Proton Colliders," SSCL-519 (1993).

71. V. Shiltsev, V. Danilov, D. Finley. A. Sery, "Considerations on Compensation of Beam-Beam Effects in the Tevatron with Electron Beams," PRST-AB 2, 071001 (1999).
72. V. Shiltsev, "Status of Beam-Beam Compensation with TEL," Proc. Beam-Beam Workhop 2003, Montauk, in conjunction with HALO'03 Workshop, to be published.
73. G. Burtin, J.-P. Koutchouk, Y. Papaphilippou, F. Roncarolo, T. Sen, V. Shiltsev, J. Wenninger, F. Zimmermann, SPS Machine Study 29.07.2004, unpublished (2004).
74. C. Carli, M. Chanel, "New Methods to Create Hollow Bunches," CERN/PS 2002-035 (AE) and Proc. 20th ICFA Advanced Beam Dynamics Workshop on High Intensity High Brightness Hadron Beams, Fermilab (2002).
75. H. Damerau, R. Garoby, "Proposal for the Creation and Storage of Long Bunches in the LHC," EPAC 2004 Lucerne (2004).
76. V.M. Juravlev, et al., "Investigations of Power and Spatial Correlation Characteristics of Seismic Vibrations in the CERN LEP Tunnel for Linear Collider Studies," CERN-SL/93-53 (1993).
77. T. Sen, J. Ellison, "Diffusion due to Beam-Beam Interaction and Fluctuating Fields in Hadron Colliders," PRL 77, 6, p. 1051 (1996).
78. J. Strait et al., "Towards a New LHC Interactin Region Design for a Luminosity Upgrade," PAC 2003 Portland (2003).
79. K. Akai, Y. Morita, "Crab Cavity for High-Current Accelerators," KEK-Preprint-2003-123 (2003).
80. "KEKB B-Factory Design Report," KEK Report 95-7 (1995).
81. G. Rumolo, F. Zimmermann, "Electron Cloud Instability with Space Charge or Beam Beam," Contribution of the SL-AP Group to the Two-Stream Instability Workshop, KEK, Tsukuba, September 11-14, and CERN-SL-2001-067 AP (2001).
82. K. Ohmi, A. Chao, "Combined Phenomena of Beam-Beam and Beam-Electron Cloud Effects in Circular e+e- Colliders", Proceedings of ECLOUD'02, Geneva 15-18 April, 2002, CERN-2002-001 (2002).
83. J. Poole, F. Zimmermann (eds.), Proc. Workshop on 'Beam-Beam Effects in Large Hadron Colliders' (LHC99), CERN, Geneva, CERN-SL-99-039-AP (1999).
84. T. Sen, M. Xiao (eds.), Proc. Workshop on 'Beam-Beam Effects in Circular Colliders', Fermilab, Batavia, June 2001, FERMILAB-CONF-01-390 (2002).

2.4 Beam-beam phenomena in the Tevatron

T. Sen, Fermilab
mail to: tsen@fnal.gov

2.4.1 Introduction

Protons and anti-protons in the Tevatron circulate on separated helical orbits within the same beam pipe and collide at two experimental detectors CDF and D0. Electrostatic separators placed at several locations create these helical orbits. In Run I there were six bunches per beam. In Run II, which started in April 2001, each beam has three trains of twelve bunches. Consequently there are six times as many long-range beam-beam interactions as in Run I. It was anticipated and observed that these long-range beam-beam interactions would have a more serious impact on beam lifetime and losses. Table 1 contains a brief list of the important parameters.

Table 1. Selected beam parameters in the Tevatron

Parameter	Injection $(p/\bar{p})$	Collision $(p/\bar{p})$
Circumference [m]	6283.187	
Number of bunches	36	
Bunch spacing [nsec]	396	
Energy [GeV]	150	980
Beta* at IP [m]	1.6	0.35
Normalized transverse emittance (95 %)[πmm-mrad]	20/15	
Bunch intensity ($\times 10^{11}$)	2.5/0.36	
Bunch length [cm]	80	48
Beam-beam parameter	0.0018/0.0092	

After a slow start partly due to the impact of the long-range interactions, the luminosity in Run II has been steadily increasing over time. Figure 1 shows the luminosity evolution over the past few years.

In 2004, the Tevatron surpassed the luminosity goals set for the 1st stage of Run II. The record until now was set on July 16, 2004 when the average initial luminosity exceeded $10^{32}\,\mathrm{cm}^{-2}\,\mathrm{sec}^{-1}$. Several improvements in the injectors and the Tevatron made this possible, see Reference [1] for more details.

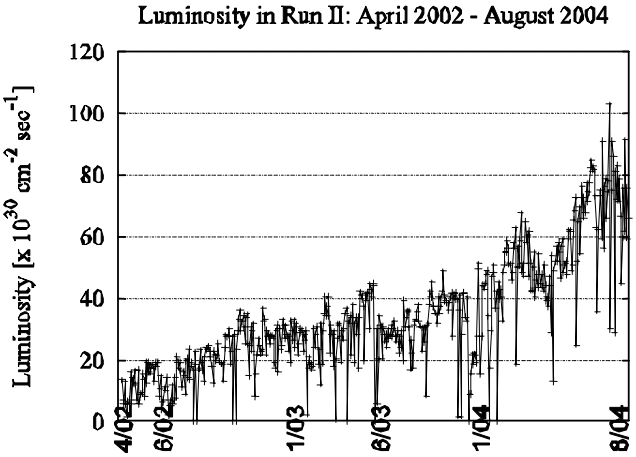

Figure 1. Evolution of the initial luminosity (averaged over CDF and D0) in Run II.

A collider fill starts with coalesced proton bunches from the Main Injector loaded one bunch at a time onto the central orbit in the Tevatron. The electrostatic separators are powered after all 36 proton bunches are loaded and the protons are moved to their helical orbit. Anti-protons are loaded four bunches at a time into one of three abort gaps onto the anti-proton helical orbit. The anti-proton bunches are moved longitudinally relative to the proton bunches ("cogged") to make room for the next four bunches in the abort gap. After each train is full the two beams are accelerated to top energy. A final cogging is done at the end of the acceleration. The optics is changed to lower the beta

functions at the IPs from 1.6m to 0.35m. After the final step of this beta squeeze, the transverse separations at the IPs are reduced to zero with the use of the appropriate separators around the IPs. Collimators are moved in to reduce the beam halo and background in the detectors and a store begins.

The configuration of beam-beam interactions is different at injection and collision. Each bunch experiences 72 long-range interactions at injection but at collision there are 70 long-range interactions and two head-on collisions per bunch. In total there are 138 locations around the ring where beam-beam interactions occur. The sequence of 72 interactions out of the 138 interactions is different for each bunch, hence the effects are different from bunch to bunch. The locations of these interactions and the beam separations change from injection to collision. The left plot in Figure 2 shows the separations at all 138 interaction points in the ring after the 2nd cogging at injection. The minimum separation is about 4σ. The right plot in this figure shows the beam separations at collision. The head-on collisions occur at B0 (CDF experiment) and D0 (D0 experiment). The minimum separations ($\sim 5\sigma$) at the parasitic encounters occur close to the experiments.

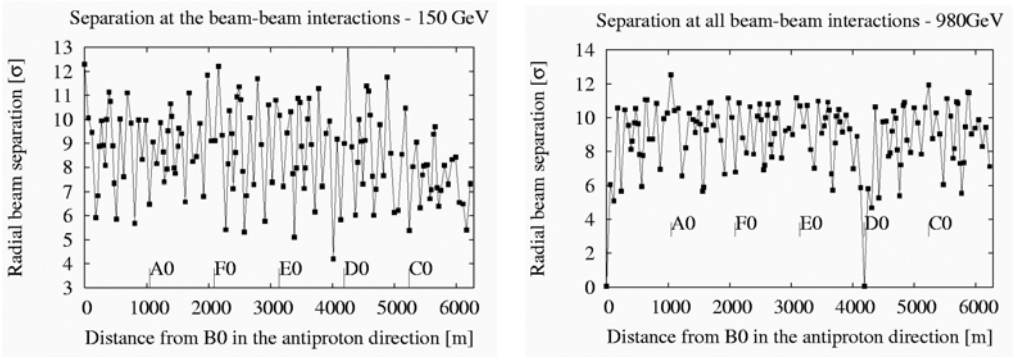

Figure 2. Left: Radial beam separations at 138 interaction points around the ring. Left: At injection (150 GeV) after the second cogging. Right: At low-beta (980 GeV). The head-on collisions are at locations B0 and D0.

2.4.2 Theory and Observations

Head-on beam-beam interactions are often characterized by a single parameter - the head-on beam-beam tune shift. This is the tune shift of a small transverse amplitude particle and it is also a measure of the beam-beam induced tune spread in the bunch. These head-on interactions drive only even order resonances so the tunes in colliders are chosen such that the tune footprint does not straddle low even order resonances. While much is understood about head-on interactions, several phenomena lack quantitative predictions, e.g. emittance growth with mismatched beams. Long-range interactions are more complex than the head-on interactions. In addition to changing the tunes, these interactions in general also change the orbits, coupling and chromaticity. As with the tune changes, the orbit, coupling and chromaticity changes are amplitude dependent. The long-range interactions drive both even and odd order resonances. The changes in orbits, tunes, coupling, chromaticity, resonance strengths depend on several parameters including: beam separations, plane of the helix, beam emittance, beta functions,

dispersion, phase advances between the interactions etc. If for example, the phase advances between the parasitics can be adjusted with independently powered quadrupoles as is done in CESR, then the resonance strengths can be significantly altered. Quadrupoles in the Tevatron are on the same bus as the main dipoles, thus ruling out that option. Instead the most direct way of minimizing the impact of the long-range interactions in the Tevatron is by manipulating the helix configuration, lower beam emittances, reduction of chromaticities and careful control of the tunes of both beams.

A first step is understanding how quantities like tune shifts, coupling, chromaticity, resonance strengths depend on beam parameters. Detailed discussions may be found in Reference [2]. For illustrative purposes it is useful to consider round beams for which the expressions simplify. The tune shifts, the strength of the coupling resonance and chromaticity shifts at small amplitudes due to a single long-range beam-beam interaction where the separations are large (compared to the beam size), the beams are round and $\beta_x = \beta_y$ are given by

$$\Delta\nu_x(0,0) = \frac{N_p r_p}{2\pi\varepsilon_p^N}\frac{\cos 2\theta}{d^2} \tag{1}$$

$$F_{1,-1,p}(0,0) = -\frac{N_p r_p}{\pi\varepsilon_p^N}\frac{\sin 2\theta}{d^2}\exp[i(\psi_x - \psi_y - (\nu_x - \nu_y - p)\frac{s}{R})] \tag{2}$$

$$\nu'_x(0,0) = 2\frac{N_p r_p}{\pi\varepsilon_p^N}\frac{1}{d^3}[\bar{\eta}_x\cos 3\theta + \bar{\eta}_y\sin 3\theta] \tag{3}$$

Here N_p is the proton bunch intensity, r_p is the classical proton radius, ε_p^N is the normalized proton emittance, θ is the angle of the plane of the helix, d is the beam separation in units of the rms proton beam size, ψ_x, ψ_y are the phase advances, ν_x, ν_y are the tunes and $\bar{\eta}_x, \bar{\eta}_y$ are the dispersions in units of the rms beam sizes. At large distances, both the tune shift and the coupling fall as $1/d^2$ while the chromaticity falls off more rapidly as $1/d^3$. The energy dependence is contained mainly in the scaled distance d. If there were enough separator strength to keep the physical separation between the two beams constant at different energies, then $d \propto \sqrt{E}$ and the above parameters would decrease with energy. If instead the scaled separation d is kept constant, as is done during the acceleration from 150 GeV to ~500 GeV, the above parameters are independent of energy. At energies above 500 GeV, the separator voltages stay at constant values close to their maximum. Consequently d decreases as $1/\sqrt{E}$ and the parameters increase with energy. These optical parameters have different dependencies on the helix angle θ. For example at 45°, the tune shift vanishes but the coupling is a maximum. If the vertical dispersion is zero, the chromaticity vanishes only if $\theta = 30^\circ, 90^\circ$.

From analytical calculations we find that at 150 GeV, the tune shifts and coupling due to the beam-beam interactions are much smaller than due to the machine nonlinearities. Chromaticity and resonance strengths are however significant. At low-beta and 980 GeV, the tune shift (and spread) and resonance strengths are dominated by the contributions of the beam-beam interactions. Effects due to synchro-betatron

resonances are important because of the large momentum spread in the beams and relatively large chromaticities. These resonances are individually of small width but are numerous and their overlap can transport particles to large amplitudes.

While these calculations yield insight, they do not provide much information on the evolution of the beams over time. Numerical simulations offer a way to follow particle motion in fields as complex as those in the Tevatron. Dynamic aperture calculations for protons and anti-protons have been done with various tracking codes, e.g. MAD, SIXTRACK, TEVLAT. Lifetime calculations for anti-protons with only beam-beam fields done by colleagues at LBNL and SLAC have also been reported earlier [3]. A simulation code BBSIM [4] has been recently developed at FNAL for calculating lifetimes, diffusion coefficients, beam profiles and emittance growth. Another code LIFETRACK developed several years ago at Novosibirsk, Russia is also being adapted for similar purposes. These lifetime codes make use of the parallel processing features now available with either PC clusters or at the NERSC supercomputing facility.

Dynamic apertures calculated by simulation were found to be in good agreement with measured dynamic apertures when the Tevatron was operated at large chromaticities of (8,8) units. Lifetime simulations at injection showed that the lifetime was sensitive to the chromaticity setting, in agreement with observations. Lifetime simulations at collision are now aimed at reproducing the observed variations in bunch to bunch lifetimes and emittance growth and finding ways to limit the effect of beam-beam interactions.

Table 2. Tevatron performance in October 2002, August 2003 and August 2004. These numbers are the averages over the respective months. The peak bunch intensities achieved during the record luminosity store on July 16th, 2004 were about 275×10^9 protons/bunch and 40×10^9 anti-protons per bunch. The data with either protons or anti-protons only were obtained during dedicated machine studies.

	10/02	08/03	08/04	pbar/p only
Maximum Luminosity $x10^{30}$	36	52	99	NA
Maximum Protons/bunch at low-beta [$x10^9$]	170	266	257	266
Maximum Pbars/bunch at low-beta [$x10^9$]	19	28	34	30
Pbar loss at 150 GeV	13%	2%	5%	2%
Proton loss at 150 GeV	14%	8%	5%	5%
Pbar loss during the ramp	8%	8%	7%	2%
Proton loss during the ramp	11%	5%	4%	3%
Pbar loss during the squeeze	2%	2%	4%	0%
Proton loss during the squeeze	2%	1%	2%	0%
Pbar lifetime at start of store [hrs]	54	30	24	900
Proton lifetime at start of store [hrs]	77	29	110	300
Pbar efficiency 150 GeV $\rightarrow$ low-beta	83%	82%	84%	96%
Proton efficiency 150 GeV $\rightarrow$ low-beta	72%	83%	89%	92%

Tevatron performance over the past two years is summarized in Table 2. We discuss beam-beam observations at each stage of the operational cycle in more detail below. Discussions of beam-beam phenomena may also be found in References [5], [6] and in several reports available on the Fermilab Accelerator Division document database [7].

2.4.3 Injection

Anti-proton losses at injection were found to be strongly influenced by beam-beam effects until recently. During most of 2002 and the first half of 2003, the anti-proton losses with protons present were much larger, ranging from 10-15%. Lifetimes ranged between 1-5 hours. The anti-proton lifetime was found to depend on the anti-proton emittance, lower emittance bunches had longer lifetimes. Experiments with only anti-protons showed that the beam loss at 150 GeV was very small, about 2%. During the summer of 2003 several changes were made which greatly reduced the anti-proton losses from around 9% to 2%. These changes included smaller longitudinal anti-proton emittances from better coalescing in the Main Injector, lowering of chromaticity following the removal of the C0 Lambertson and introduction of the transverse dampers, lower currents in some feed-down sextupole circuits which reduced strong local nonlinearities and removal of SEMs from the injection lines which reduced the emittance blow-up. Beam-beam effects at 150 GeV now have very little influence on anti-proton losses.

Proton losses at injection have not been significantly influenced by the anti-protons. Instead the proton lifetime has largely been determined by the machine chromaticity and momentum spread. After the introduction of the transverse dampers, removal of the C0 Lambertson magnet, a significant source of impedance, and the installation of a liner in the F0 Lambertson, protons could circulate stably in the Tevatron with lower chromaticities. Lowering the chromaticities from 8-10 units to 2-4 units has improved the proton lifetime at 150 GeV. The small dynamic aperture on the proton helix due to the magnet nonlinearities and restricted physical aperture at a few locations are now the main sources of beam loss. While the impact of beam-beam interactions on protons has been small, nevertheless the proton lifetime does drop while anti-protons are loaded and proton losses are observed during cogging when the beam separations change.

2.4.4 Acceleration

Anti-proton losses during acceleration are strongly influenced by beam-beam interactions. On average anti-proton losses are about 6% higher when protons are present. The losses are observed to be well correlated with the vertical emittance, lower emittance bunches have lower losses. During the ramp the separator voltages increase linearly until about 500 GeV when the maximum voltage is reached. The beam separation, in units of the beam size, stays constant while the separator voltages are increasing but falls thereafter. As a consequence the significant portion of anti-proton losses is observed during the second half of the ramp. Helix solutions that increase the minimum separation in the last part of the ramp were commissioned in August 2003 and have lead to some improvement [8].

Proton losses during acceleration have remained around 5% over the past year. Beam studies have shown that the losses occur mostly in the early part of the ramp and depend strongly on the longitudinal emittance [9], the quality of coalescing in the Main Injector and more recently on the vertical emittance.

We expect that lowering the chromaticities during the acceleration will also help reduce losses. The use of octupoles and/or transverse dampers during the ramp will be commissioned in future beam studies. The beam separations will also be increased with additional separators.

2.4.5 Squeeze

Anti-proton losses were very large (~ 20-25%) until March 2002 during the step in the squeeze when the helix reverses polarity. At this stage, the minimum beam separation was less than 2σ. A helix solution was found that increased the beam separation at this point in the squeeze. That combined with a faster transition through this step reduced anti-proton losses significantly. Even with this helix the beam separation drops momentarily during the transition from the injection to the collision helix. There is some evidence of beam-beam related anti-proton losses (~ 2%) during the squeeze. Some of these losses occur during beam scraping done for 10 minutes after the beams are brought into collision following the squeeze. This scraping removes halo particles and results in about 1% beam loss in both beams.

Proton losses during the low-beta squeeze are usually not significant. Adjustments of the orbits and tunes have usually sufficed to control losses when they are occasionally large.

2.4.6 Collision

At collision, each bunch experiences 2 head-on collisions and 70 long-range interactions. The nominal working point ($\nu_x = 0.585$, $\nu_y = 0.575$) is chosen to lie between fifth and seventh order resonances. For anti-protons, the head-on collisions contribute a tune shift about 0.02 while all the long-range interactions contribute about 0.005. Fig. 3 shows the footprints due to the beam-beam interactions for bunch 1, 6, and 12 superposed on nearby sum resonances up to twelfth order. Footprints of bunches 2-11 are clustered around the footprint of bunch 6. The major differences in the tune shifts between bunch 6, and bunch 1 and 12 are due to the missed parasitic collision closest to the IP, upstream for bunch 1 and downstream for bunch 12. Due to the 3-fold symmetry, this pattern is repeated in the other two trains.

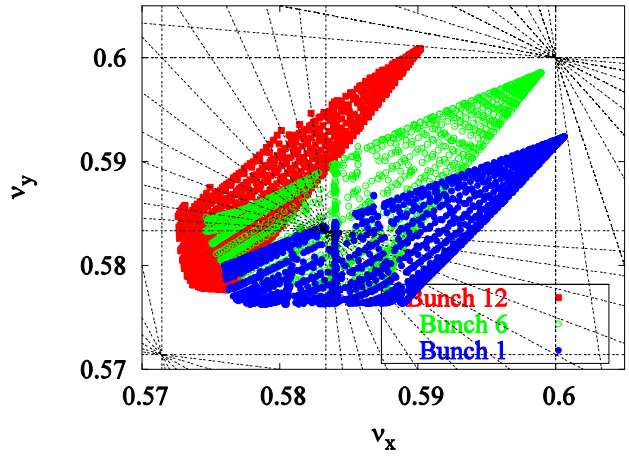

Figure 3. Tune footprint of anti-proton bunches 1, 6 and 12 in a train during collisions at 980 GeV. Sum resonances up to 12th order are also shown.

This bunch to bunch difference in tunes has now been experimentally measured in several stores with a new high frequency Schottky monitor [10]. Figure 4 shows the

bunch by bunch tunes measured in a recent store and an analytical calculation of the tune shifts [2]. This pattern of tune shifts has been reproducibly observed in several stores. The analytical results predict both the scale of the tune shifts and the variation between bunches in both planes reasonably well. The residual differences are due to uncertainties in the optics, beam intensities and emittances.

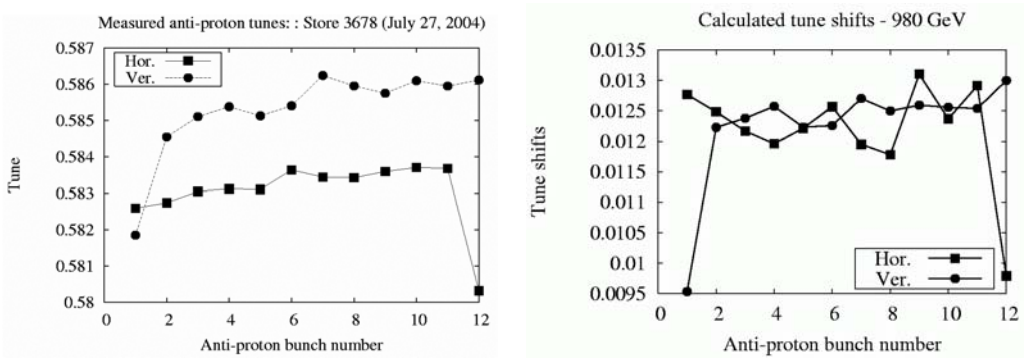

Figure 4. Left: Measured bunch by bunch tunes of anti-protons (courtesy of P. Lebrun), Right: analytical prediction of the centroid tune change within a bunch (right).

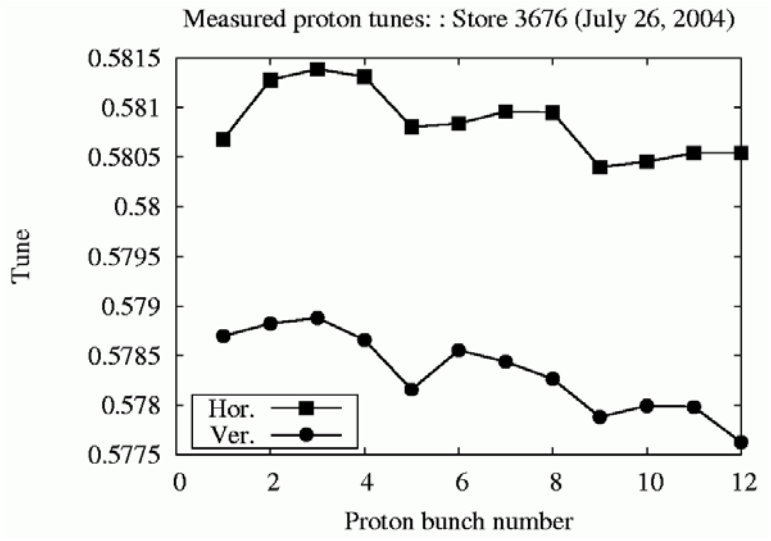

Figure 5. Measured bunch by bunch tunes of protons in a recent store (courtesy P. Lebrun).

Bunch by bunch tunes of protons were measured recently in one store - see Figure 5. While the tune variations between bunches are small, these variations could be due to beam-beam effects from the anti-protons. The pattern of tune variation, roughly periodic over 4 bunches, follows the intensity distribution of the anti-protons - see Figure 7 for an example. The tune differences are however close to the resolution of the tune measurement - more such measurements are required to definitively attribute the shifts to beam-beam effects.

The long-range beam-beam interactions also have an impact on bunch to bunch orbits. A synchrotron light monitor is able to image individual proton and anti-proton bunches at collision [11]. Figure 6 shows the orbits of anti-protons as observed in an early store.

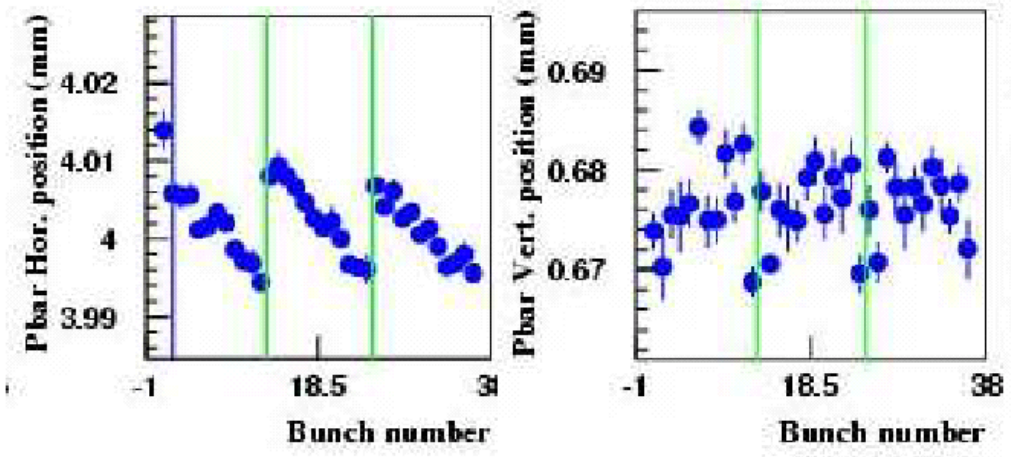

Figure 6. Positions of anti-proton bunches observed at the synchrotron light monitor in Store 1787. Long-range interactions are responsible for the differences in bunch to bunch orbits [12].

The horizontal position of the anti-proton bunches shows the same trend in all three trains - as expected from the three-fold symmetry. The maximum spread in horizontal position is about 30 microns (in the first train) and closer to 20 microns in the other trains. The vertical spread is smaller than 20 microns in all trains. The spread in proton orbits is about a factor of 2-3 smaller. The observed orbit shifts agree well with analytical calculations of these shifts [12].

We now discuss the impact on beam lifetimes and emittances with the example of a store on August 18th, 2004 - one of the recent higher luminosity stores before the shutdown in August.

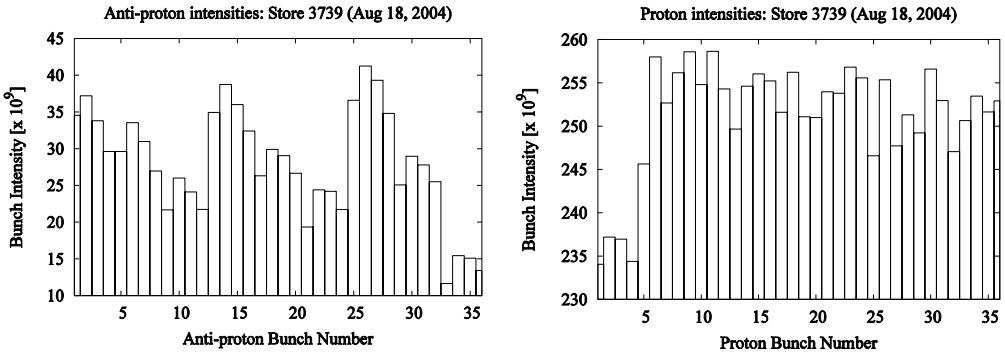

Figure 7. Bunch by bunch intensities at the start of Store 3739 (August 18, 2004). Left: anti-protons; Right: protons

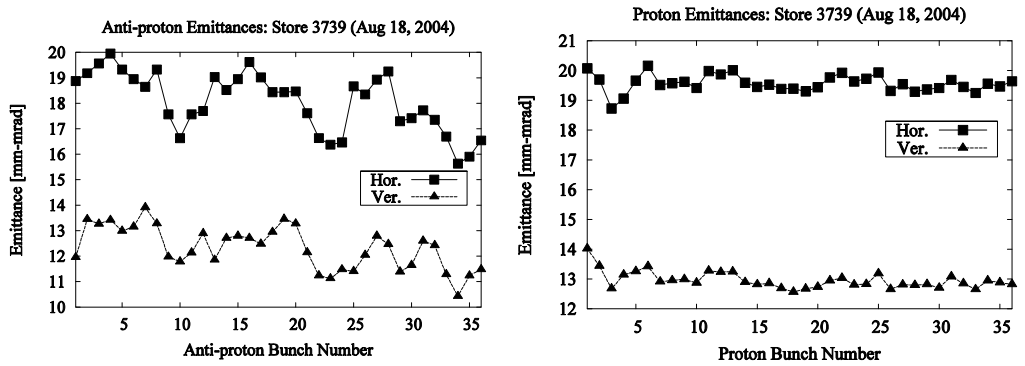

Figure 8. Bunch by bunch emittances at the start of Store 3739 (August 18, 2004). Left: anti-protons; Right: protons

Figure 7 shows the intensity distribution among the anti-proton and proton bunches in this store. Typically the average intensities of the first 4 anti-proton bunches in each train are larger than those of the following bunches in the train - these leading bunches are the first 12 anti-proton bunches to be injected. In this store the intensities of the last 4 bunches A33-A36 was particularly low, thus the intensities over the whole beam varied by a factor of 4. The intensity distribution amongst proton bunches is typically more uniform, in this store the variation is about 10%. The emittance distribution is shown in Figure 8. The last 4 anti-proton bunches in each train typically have a lower emittance than the others, the range of variation in this store is about 4π mm-mrad for the normalized 95% emittance. The proton emittance distribution is much more uniform, the range of variation is about 1π mm-mrad.

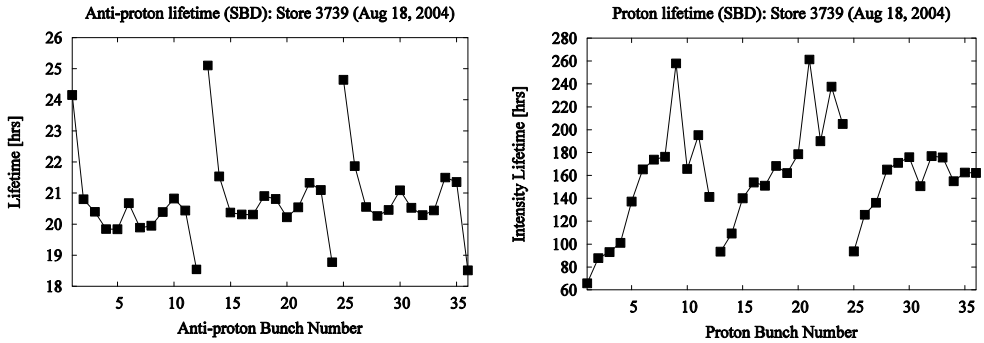

Figure 9. Intensity lifetimes, bunch by bunch, at the start of Store 3739 (August 18, 2004). Left: anti-protons; Right: protons. The gaps show the 3 trains of 12 bunches in each beam.

Figure 9 shows the bunch by bunch intensity lifetimes of both beams. This lifetime is mainly determined by the luminosity. Since the proton intensity and emittance distribution is relatively uniform, the 3-fold symmetry of the bunch structure is clearly reflected in the anti-proton lifetimes. This symmetry is somewhat broken in the lifetimes of the proton bunches. The lifetimes of the last 4 proton bunches in the first 2 trains, P9-P12 and P21-P24, are larger than those of P33-P36, the last 4 bunches in the 3rd train. This is a particular feature of this store since P9-P12 collided with the low intensity anti-proton bunches A33-A36 at D0, P21-P24 collided with these anti-proton

bunche at B0 while P33-P36 do not collide with them anywhere but instead with the higher intensity bunches A21-A24 at B0 and bunches A9-A12 at D0.

The bunch lifetime related to dynamics (i.e. not related to luminosity) can be calculated as

$$\frac{1}{\tau_{Dy}(\bar{p})} = \frac{1}{\tau(\bar{p})} - \frac{1}{\tau_{\mathcal{L}}(\bar{p})} \tag{4}$$

$$\frac{1}{\tau_{\mathcal{L}}(\bar{p})} \equiv \frac{L\sigma_{p\bar{p}}}{N_{\bar{p}}} = \frac{f_{rev}}{2\pi} \frac{N_p}{\beta^* \sqrt{(\varepsilon_{x,p} + \varepsilon_{x,\bar{p}})(\varepsilon_{y,p} + \varepsilon_{y,\bar{p}})}} H(\frac{\beta^*}{\sigma_{s,eff}})\sigma_{p\bar{p}} \tag{5}$$

Here ε are the transverse emittances, H is the hourglass factor and $\sigma_{p\bar{p}}$ is the inelastic $p-\bar{p}$ scattering cross-section. Figure 10 shows the dynamic lifetime τ_{Dy} for both beams. Variations in these lifetimes are mainly due to beam-beam effects. The 3-fold symmetry is still present in the anti-proton dynamic lifetime - the only spoiler is bunch A25 which has a significantly lower dynamic lifetime than bunches A1 and A13 at the head of the other 2 trains. The dynamic lifetime of protons varies over a large range, between 120-800 hours, perhaps indicative of beam-beam effects on the protons as well. Longitudinal losses due to intra-beam scattering and rf noise may also account for some of the differences bunch to bunch. The lifetime due to scattering off the residual gas is in the range of 600-900 hrs at 980 GeV [13].

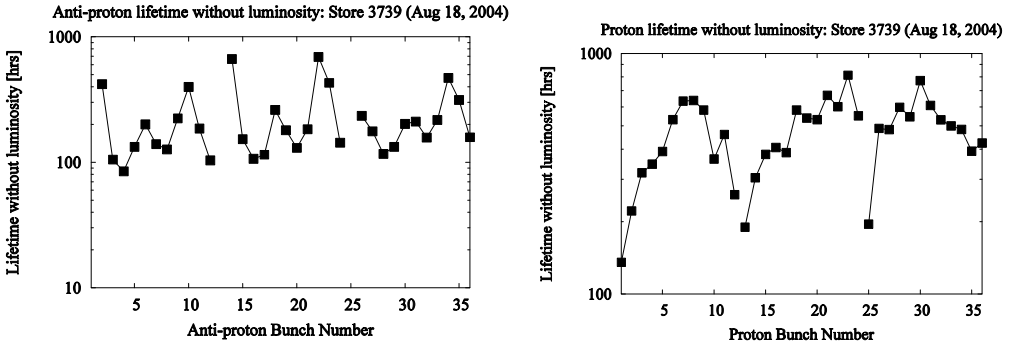

Figure 10. Lifetimes not related to luminosity losses for anti-protons (left) and protons (right). The lifetimes due to luminosity were subtracted from the intensity lifetimes as shown in Equation (4).

The transverse emittance growth times of proton bunches in this store were in the range from 14-21 hours with intra-beam scattering the dominant contributor. The anti-proton emittances grew at a much slower rate in this store. This has not always been the case. Until recently in some stores with relatively high proton intensities, large emittance growth was observed in most anti-proton bunches. The bunches at the head and tail of a train however had a lower emittance growth rate, so the emittance profile within a train had a scalloped shape - see Reference [1] for an example. This emittance growth was very sensitive to the tune setting - in recent stores, this problem seems to have been eliminated by small adjustments to the tunes.

Another clear manifestation of beam-beam effects on anti-protons is observed in the change of tunes during the store. The tunes change because of the intensity loss and

emittance growth of the opposing beam. From the expression for the head-on tune shift, it follows that the rate of tune change of anti-protons, for example, is

$$\frac{d}{dt}\Delta\nu(\bar{p}) = -\xi(\bar{p})(\frac{1}{\tau_{\varepsilon_p}} + \frac{1}{\tau_p}) \tag{6}$$

where $\xi(\bar{p})$ is the beam-beam parameter for anti-protons, τ_{ε_p} is the proton emittance growth time and τ_p is the proton intensity lifetime. The proton emittance growth has a larger impact on the anti-proton tune change because $\tau_{\varepsilon_p} < \tau_p$. Conversely, the rapid intensity loss of anti-protons contributes more than the anti-proton emittance growth to the proton tune change.

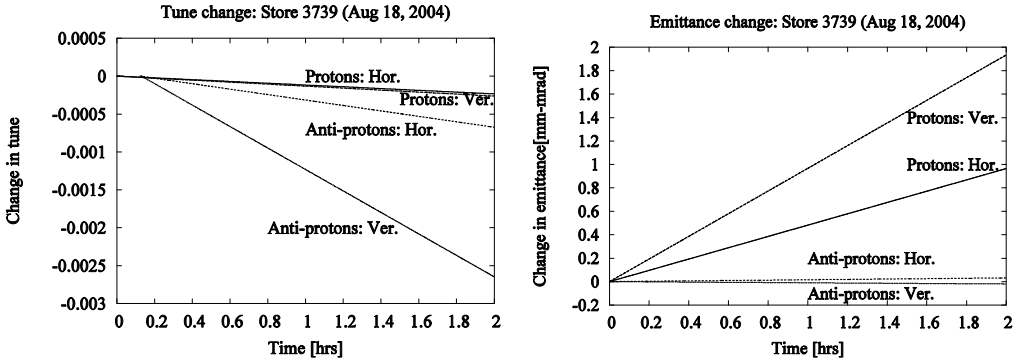

Figure 11. Changes in the average tunes(left) and emittance(right) during the first 2 hours of the store. The beam-beam related tune changes are related to the changes in the intensity and emittance of the opposing beam. For example, the larger anti-proton tune changes are well correlated with the larger growth of the proton emittances.

The left panel in Figure 11 shows the tune changes averaged over all bunches for both beams. The right panel in this figure shows the average emittance change over this same time. The fact that the anti-proton tune changes are larger correlates well with the larger emittance change of the protons.

A recent phenomenon with smaller anti-proton emittances and increasing anti-proton intensities has been the occasional large proton losses at the start of stores. These large losses were enough to significantly increase the background in the detectors. Analysis showed that typically proton bunches that collided with anti-proton bunches with the smallest vertical emittance had the largest losses. This suggests that losses are due to those protons which see the strongest part of the non-linear beam-beam force. These losses are also very tune dependent. Recently the proton tunes were placed between the 7th and 12th order resonances with the differential tune circuits. These changes have brought the initial proton losses under control.

2.4.7 Beam-beam compensation

Tevatron Electron Lens (TEL)

The TEL has been in operation since March 2001 and aims to compensate the tune spread between bunches at top energy. The electron gun was replaced in Janurary 2003 by another gun which creates a smoother Gaussian profile of the electron beam. In

studies with the electron lens acting on protons, the smoother field was found to preserve the lifetime of the protons and was a significant improvement over the previous gun which created a more rectangular profile. The alignment of the lens is very critical - for example the sign of the induced tune shift can change due to small changes in the orbit. In a beam study performed in a store where scallops had developed, the electron lens was successfully used to change the tuneshift of a selected anti-proton bunch and thereby reduce its emittance growth rate. The electron lens is also routinely used to remove coasting protons circulating in the ring by resonant excitation of particles in the abort gaps. It has also been used on occasion to tickle a bunch to increase the signal to noise ratio for a tune measurement. Further work on the electron lens to make it an operational device for tune shift compensation is continuing. The improvements required include better control of the electron lens orbit, improved stabilization of electron currents and perhaps a wider electron beam. More details can be found in Reference [1].

Wire Compensation

Compensation of the long-range interactions by steady current carrying wires was investigated for the Tevatron following a similar proposal for the LHC [14]. A preliminary investigation with four 1m long wires placed in four warm straight sections showed that the dynamic aperture of a selected anti-proton bunch at 150 GeV could be significantly increased by appropriate placement of the wires and carefully selected currents. More recent investigations at collision energy [15] showed that the wire compensation works only in ideal cases, e.g. when the beams are round and the wire can be placed at nearly the same betatron phase as the beam-beam interaction. The beams are not round at several of the long-range interactions in the Tevatron. In fact, the beams are highly elliptical (aspect ratio 4:1) at the parasitics closest to the IPs. These interactions cannot be well compensated with the field of round wires. Wires with elliptical cross-sections could be an alternative. However this project has been dropped from the Run II upgrade given its R& D nature and the limited time scale of Run II.

2.4.8 Summary

Observations over the last few years of Run II have shown that the important parameters that can control the impact of beam-beam interactions are: smooth helices (too small or too large beam separations need to be avoided), small beam emittances, low machine chromaticity, proper choice of machine tunes, and low machine coupling.

Transfer efficiencies in the Tevatron at the start of Run II were severely limited by beam-beam effects. The major losses were those of anti-protons during the squeeze. Smaller but significant anti-proton losses also ocurred at 150 GeV and during acceleration. Most of these losses were overcome by changing the helices to increase the beam separations, with smaller anti-proton emittances and by operating at lower chromaticities. Large proton losses and large emittance growth of anti-protons at the start of stores have been corrected mainly by adjustments of the tunes. At present beam-beam related losses reduce the integrated luminosity by 16-24%: 2% due to losses at 150 GeV, 6-8% during acceleration and squeeze, and 8-16% due to losses at the start of collisions. There is therefore room for further improvement, especially during the acceleration and during the early part of a store.

Anti-proton intensities are expected to increase about 3-4 fold during the Run II upgrade. Strong-strong effects due to the beam-beam interactions could start to become important. Careful control of beam losses at all stages of the Tevatron operational cycle will continue to be required.

Understanding and mitigating the effects of the beam-beam interactions in the Tevatron has been made possible by the dedicated work of several colleagues including (but not limited to): Y. Alexahin, J. Annala, B. Erdelyi, N. Gelfand, A. Jansson, J. Johnstone, V. Lebedev, P. Lebrun, M. Martens, R. Pasquinelli, R. Moore, V. Shiltsev, D. Still, M. Syphers, C.Y. Tan, A. Tollestrup, A. Valishev, M. Xiao, X.L. Zhang (at Fermilab), and F. Schmidt, F. Zimmermann (at CERN) as well as colleagues at BNL, LBL and SLAC.

2.4.9 References

1. V. Shiltsev, Proceedings of EPAC 2004
2. T. Sen, B. Erdelyi, M. Xiao, V. Boocha, *Beam-beam effects at the Fermilab Tevatron: theory*, PRSTAB , 041001 (2004)
3. A. Kabel et al. Proceedings of PAC03, pg 3542,
   J. Qiang et al., Proceedings of PAC03, pg 3401
4. `http://waldo.fnal.gov/tsen/BBCODE/public/`
5. T. Sen, Proceedings of PAC 2003, pg 34
6. X.L. Zhang et al., Proceedings of PAC 2003, pg 1757
7. `http://beamdocs.fnal.gov`
8. Y. Alexahin, FNAL report Beams-doc-802-v1 (2003)
9. T. Sen et al., Proceedings of PAC 2003, pg 1754
10. R.J. Pasquinelli et al., Proceedings of PAC 2003, pg 3068,
    A. Jansson et al., Proceedings of EPAC 2004,
    P. Lebrun, FNAL report Beams-doc-1275-v1 (2004)
11. H. Cheung et al, Proceedings of PAC 2003, pg 2488
12. T. Sen, FNAL report Beams-doc-689 (2003)
13. A. Tollestrup et al., Proceedings of PAC 2003, pg 2497
14. J.P. Koutchouk, LHC Project Note 223 (2000),
    J.P. Koutchouk, J. Wenninger and F. Zimmermann, Proceedings of EPAC 2004
15. B. Erdelyi and T. Sen, FNAL report Fermilab-TM-2268-AD (2004)

2.5 Beam-Beam Effects in the Relativistic Heavy Ion Collider

Wolfram Fischer and Rogelio Tomas, BNL
mail to: Wolfram.Fischer@bnl.gov and rtomas@bnl.gov

2.5.1 Introduction

The beam-beam interaction is a major consideration in the operation of the Relativistic Heavy Collider (RHIC). It can lead to emittance growth and particle loss, and is a source for experimental background. Machine parameters, close to the maximum parameters achieved so far, are presented in Table 1. The p-p parameters used in operation differ from those shown in the Table. So far the bunch intensity was limited to $0.7 \cdot 10^{11}$ due to polarization requirements.

RHIC consists of two superconducting rings, Blue and Yellow, and has produced gold-gold, proton-proton and deuteron-gold collisions. With RHIC's interaction region design (Figure 1) and with 4 experiments beams experience 4 head-on, and 2 long-range collisions per turn. The long-range interactions are with at least 7 rms beams sizes separation. With 120 or less bunches per ring (the current limit), sets of 3 bunches in one ring and 3 bunches in the other ring are coupled through the beam-beam interaction.

Table 1: Latest machine parameters relevant to beam-beam interactions, for Au-Au and p-p collisions.

Parameter	Unit	Au-Au	p-p
relativistic γ, injection	…	10.5	25.9
relativistic γ, store	…	107.4	106.6
no of bunches, n_b	…	45	28
ions per bunch, N_b	10^9	1.1	170
emittance $\varepsilon_{N\ x,y\ 95\%}$	mm·mrad	10	20
chromaticities (ξ_x,ξ_y)	…	(+2,+2)	
harmonic no h, store	…	7×360	360
synchrotron tune Q_s	10^{-3}	3.0	0.5
rms bunch length σ_z	m	0.3	0.7
rms momentum spread σ_p/p		0.15	0.3
envelope function β^* at IP	m	1-10	
beam-beam ξ/IP	…	0.0025	0.007
head-on collisions	…	4	2
parasitic collisions	…	2	4

Two beam splitting DX dipoles are the magnets closest to the interaction point (IP). They are each 10m away from the IP (Figure 1). Beams collide nominally without a crossing angle. With rf manipulations, the crossing point can be moved longitudinally. If the bunch spacing is large enough (with 60 or less bunches per ring), it is possible to separate the beams longitudinally and switch off all 6 beam-beam interactions.

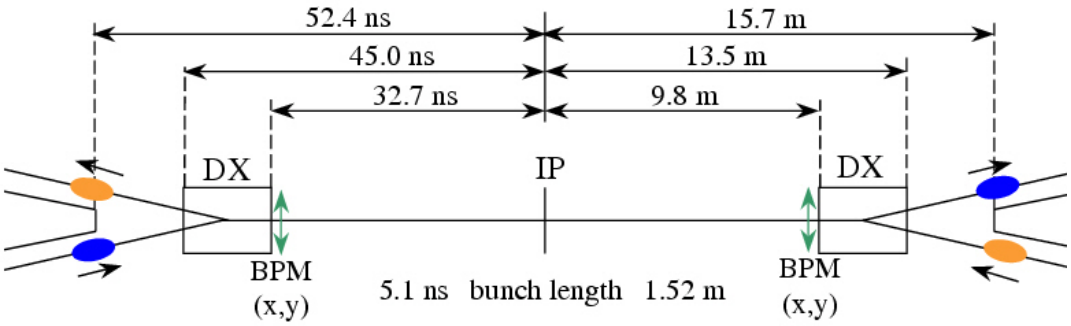

Figure 1: RHIC interaction region. Beams share a common beam pipe between the splitting DX dipoles. The bunch spacing shown corresponds to a fill pattern of 120 symmetrically distributed bunches.

Beam-beam phenomena observed in other hadron colliders [1] can also be seen in RHIC. In addition, with bunches of equal intensity the beams are subject to strong-strong effects. To accommodate acceleration of different species, the two RHIC rings have independent rf systems. With different rf frequencies the beam-beam interaction is modulated and can have a visible impact on the beam lifetime. The overview presented here is a summary of material presented in Refs. [2,3].

2.5.2 Quest for a new Working Point

Changing the working point is a strategy to alleviate the beam-beam effect and improve the performance of the machine. We considered as candidates for a new working point those of other hadron colliders. Those working point not suitable to host polarized beams were discarded.

Testing new working points at top energy represents a very significant effort since it requires the set-up of an energy ramp, which can take shifts of dedicated operation. Since the beam-beam parameter does not depend on the energy or the β-functions at the interaction point, the beam-beam effect can also be studied at injection.

The beam-beam interaction is not the only effect that strongly affects the beam dynamics. The magnetic non-linearities present in the interaction regions considerably reduce the dynamic aperture of the lattice. The dynamic aperture was estimated for these different working points by tracking particles for one million turns including the beam-beam interaction in the weak-strong approximation. Experiments to assess beam-beam effects at injection were performed with gold ions during the 2004 gold operation. Each beam consisted of 56 bunches with about $0.7 \cdot 10^9$ Au^{79+} ions. The beam decay rate was measured with and without collisions by fitting the wall current monitor intensity curve at the different tunes. Collisions were set at two interaction points (the STAR and PHENIX experiments). The results for the two most relevant working points are shown in Figure 2.

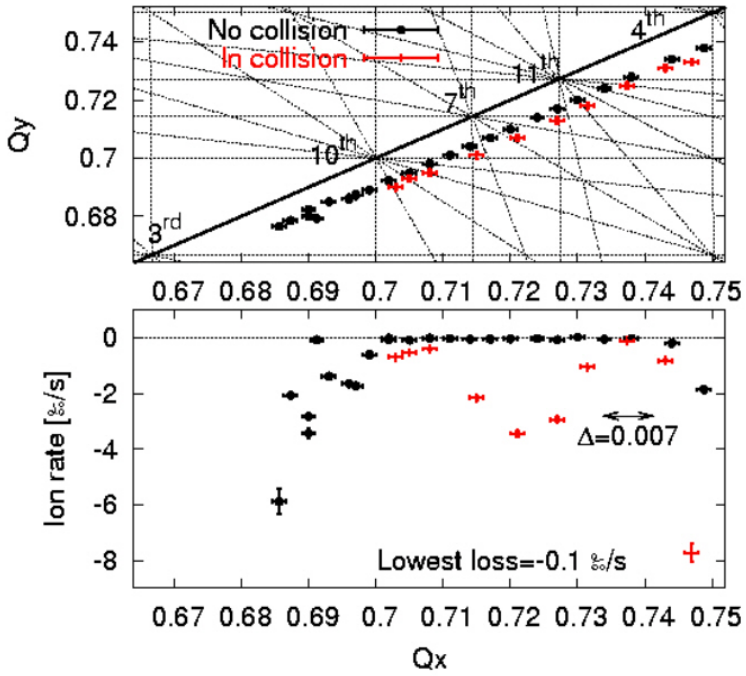

Figure 2: Tune scan at injection

The beam lifetime near the SPS collider tunes of 0.68 is very short due to the proximity of the third order resonance. Instead a good working range around 0.73 was found at injection. This does not imply that at store the SPS tunes are worse than the other. Indeed the prediction of the dynamic aperture at store is shown in Figure 3.

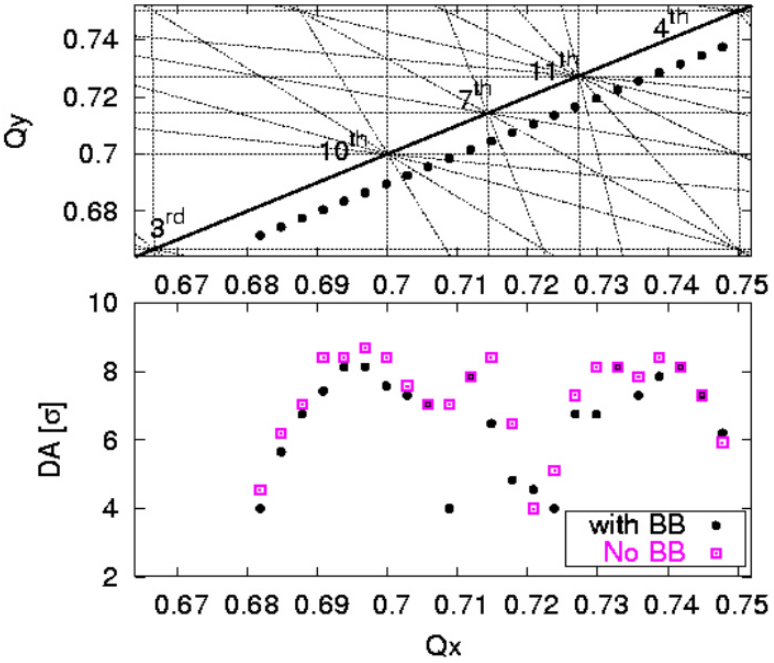

Figure 3: Tune scan and simulation at store.

With the beam-beam interaction, the dynamic aperture of the two possible working points is slightly larger than 8 transverse rms beam sizes. Therefore both tunes should be suitable for operation. During the 2004 proton operation both tunes were used. The SPS collider tunes performed slightly better in terms of beam lifetime, and significantly better in terms of beam polarization.

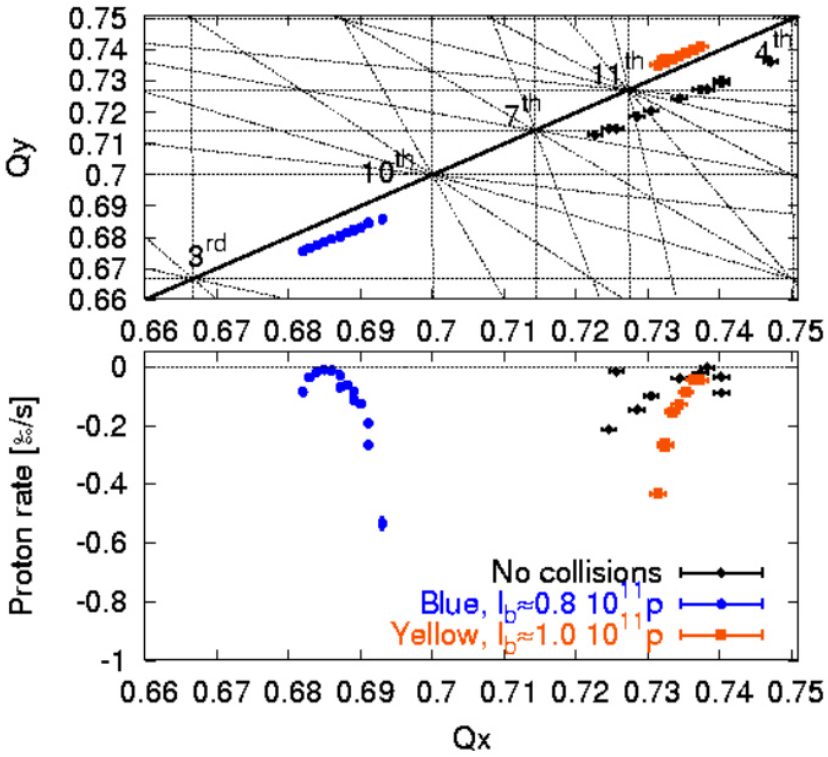

Figure 4: Tune scans at store with 4 head-on collisions.

During the proton run, a beam-beam parameter of $\xi = 0.004$/IP was reached with 4 head-on collisions, and a beam-beam parameter of $\xi = 0.007$/IP with only 2 head-on collisions.

2.5.3 Strong-Strong Observations

RHIC sees strong-strong beam-beam effects. In addition to the tune (σ-mode) a new transverse oscillation mode (π-mode) occurs. For a single collision per turn the π-mode is at a tune $Y\xi$ below the σ-mode, where $Y \approx 1.2$ for round beams [4]. If the beam-beam interaction is the dominant nonlinear effect, the π-mode can be outside the continuous spectrum and thus be undamped [5].

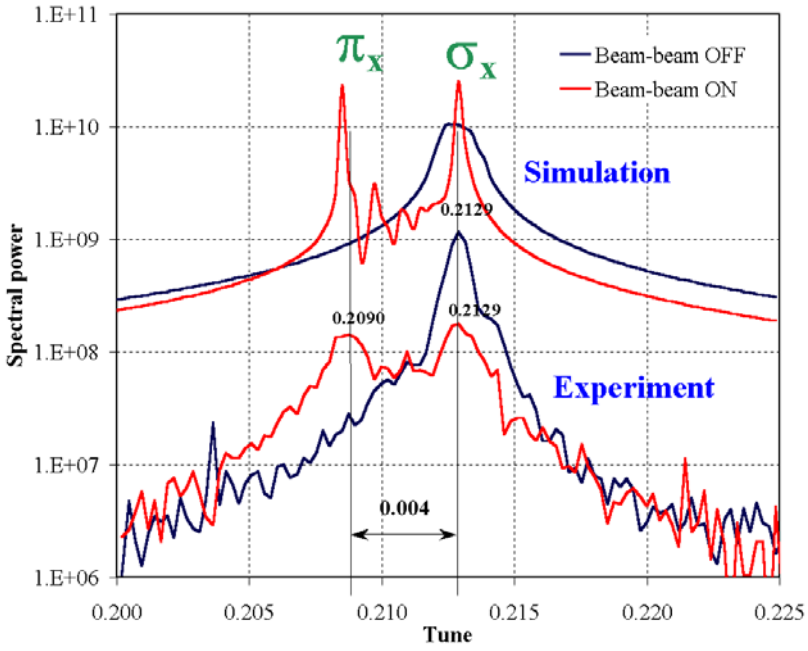

Figure 5: Coherent dipole modes in an experiment with a single proton bunch per beam, and a corresponding simulation [65]. $\xi = 0.003$, spectra from 4096 turns.

Coherent beam-beam modes were observed in an experiment with proton beams, with a beam-beam parameter $\xi = 0.003$ and a single collision per turn (Figure 5). The measured difference between the σ- and π-modes is consistent with a Yokoya factor of $Y \approx 1.2$. The locations of the π-modes were reproduced in a strong-strong simulation [7]. π-modes were also observed in routine operation with a beam-beam parameter $\xi = 0.0015$, four collisions per turn and linear coupling (Figure 5). The π-modes could be suppressed by small changes in one of the tunes. So far, coherent modes have not negatively impacted the collider operation.

2.5.4 Unequal RF Frequencies

When the two RHIC beams have different radio frequencies f_{rf} the beam crossing points move longitudinally with the speed

$$v_{CP} = \frac{c}{2}\frac{\Delta f_{rf}}{f_{rf}}$$

where c is the particle speed. Values of $\Delta f_{rf} = 5$Hz and $v_{CP} = 27$m/s were typical with gold beams in both rings, during the ramp. When deuteron and gold beams were injected with the same rigidity in 2002 [8], $\Delta f_{rf} = 44$kHz is needed and $v_{CP} = 3$m/turn. Beams experience the beam-beam interaction only when the crossing point is between the DX magnets (Figure 6). With slowly moving crossing points (gold-gold case) the beam-beam interaction is modulated, with fast moving crossing points (deuteron-gold case) beams experience pseudo random interactions in time.

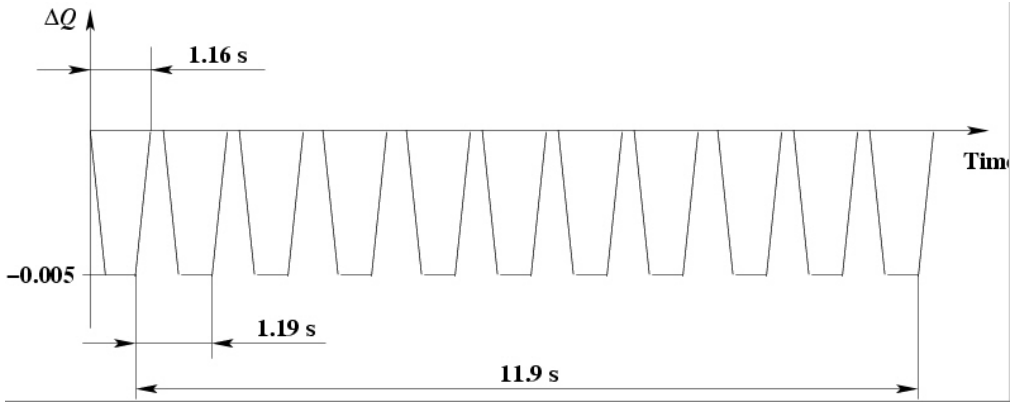

Figure 6: Tune modulation of particles in the centre of a bunch due to moving collision points, for Δf_{rf} = 5Hz, no crossing angle, 60 bunches and a total beam-beam tune shift of ΔQ_{tot} = -0.005.

Slowly moving crossing points and head-on collisions lead to tune modulation and to unacceptable beam lifetime [9]. The tune modulation depth is determined by the beam-beam parameter, the modulation waveform by the crossing angle, and the modulation frequency by the fill pattern and the difference in the rf frequencies Δf_{rf}. Figure 6 shows a case typical for gold-gold operation. To avoid this unwanted effect, the rf frequencies are now locked during ramps. This is challenging for ion beams that have to cross the transition energy.

2.5.5 Spin Effects and Future Upgrades

The effect of the beam-beam interaction on the beam polarization of proton beams was studied earlier with simulations of up to 10000 turns [10,11,12]. In these studies, no detrimental effect of the beam-beam forces on the proton beam polarization was found. This is in agreement with observations so far.

Studies are under way to implement electron cooling in RHIC [13]. To enhance the luminosity, electron cooling may create a dense beam core that is surrounded by beam of lesser density, forming a bi-Gaussian transverse distribution. The beam-beam interaction under these conditions is being studied. A possible way to mitigate beam-beam effects may be to shape the transverse beam profiles of the colliding beams with variable profiles of the electron beams used for cooling.

The proposed electron-ion collider eRHIC [13] would be a collider with two rings of different circumference. In the electron ring a beam-beam parameter of up to 0.08 needs to be accommodated. Studies to date indicate that this can be done [14].

An increase in the RHIC luminosity by an order of magnitude may be implemented with superbunches [15]. Superbunches, however, would require a major upgrade in the timing system of the detectors. This may be easier to accommodate with a new detector [16]. A number of effects that are associated with superbunches need to be studied in more detail.

2.5.6 Summary

The beam-beam interaction has a significant impact on lifetime and emittance of the RHIC beams. Recent work shows that a change of the working point from (0.22,0.23) to (0.68,0.69) would allow the accommodation of a larger beam-beam parameter.

In addition to beam-beam effects observed in other hadron colliders, coherent beam-beam modes were seen for the first time. With independent rf systems for both rings, differences in the rf frequencies can lead to tune modulation and emittance growth. Beam-beam work relating to future upgrades, electron cooling and eRHIC, has started.

2.5.7 Acknowledgements

The author would like to acknowledge discussions with and support from Y. Alexahin, M. Bai, M. Blaskiewicz, M. Brennan, M. Furman, C. Montag, S. Peggs, J. Qiang, T. Roser, T. Sen, S. Tepikian, J. van Zeijts, and F. Zimmermann.

2.5.8 References

1. S. Saritepe, G. Goderre, and S. Peggs, “Observations of the Beam-Beam Interaction in Hadron Colliders”, in “Frontiers of Particle Beams: Intensity Limitations”, Springer-Verlag, Lecture Notes in Physics (1991).
2. W. Fischer, M. Blaskiewicz, J.M. Brennan, P. Cameron, R. Connolly, C. Montag, S. Peggs, F. Pilat, V. Ptitsyn, S. Tepikian, D. Trbojevic, and J. van Zeijts, "Observation of Strong-Strong and Other Beam-Beam Effects in RHIC", proceedings of the 2003 Particle Accelerator Conference, Portland, Oregon (2003).
3. R. Tomas, M. Bai, W. Fischer, V. Ptitsyn, T. Satogata, and T. Roser, "Quest for a New Working Point in RHIC", proceedings of the 2004 European Particle Accelerator Conference, Lucerne, (2004).
4. K. Yokoya and H. Koiso, “Tune Shift of Coherent Beam-Beam Oscillations", Part. Accel. Vol. 27, pp. 181-186 (1990).
5. Y. Alexahin, “On the Landau Damping and Decoherence of Transverse Dipole Oscillations in Colliding Beams”, Part. Accel., **V59**, p. 43; CERN-SL-96-064 (AP) (1996).
6. J. Qiang, M. Furman, R.D. Ryne, W. Fischer, T. Sen, and M. Xiao, "Parallel Strong-strong/Weak-strong Simulations of Beam-beam Interactions in Hadron Accelerators", proceedings of the 2003 Beam-Beam Workshop, Montauk, New York (2003).
7. M. Vogt, J.A. Ellison, W. Fischer, and T. Sen, "Simulations of Coherent Beam-Beam Modes at RHIC", proceedings of the 2002 European Particle Accelerator Conference, Paris (2002).
8. W. Fischer, “Run Overview of the Relativistic Heavy Ion Collider”, http://www.rhichome.bnl.gov/RHIC/Runs/.
9. W. Fischer, P. Cameron, S. Peggs, and T. Satogata, "Tune modulation from beam-beam interaction and unequal radio frequencies in RHIC", proceedings of the 2003 Beam-Beam Workshop, Montauk, New York (2003).
10. Y. Batygin and T. Katayama, "Beam-Beam Simulation at RHIC", BNL Spin Note AGS/RHIC/SN No. 052 (1997).

11. Y. Batygin and T. Katayama, "Numerical Study of Spin Depolarization in RHIC Due to Beam-Beam Collision", BNL Spin Note AGS/RHIC/SN No. 053 (1997).
12. A. Luccio and M. Syphers, “Effects of Beam-Beam Interaction on Spin Motion”, BNL Spin Note AGS/RHIC/SN No. 068 (1997).
13. T. Hallman, T. Kirk, T. Roser, R.G. Milner, “RHIC II/eRHIC White Paper”, submitted to NSAC Sub-Committee on Future Facilities (2003).
14. C. Montag, "Beam-Beam Studies for the Electron-Ion Collider eRHIC", BNL C-A/AP/155 (2004).
15. W. Fischer and M. Blaskiewicz, "Luminosity increase at the Incoherent Beam-Beam Limit with Six Superbunches in RHIC", proceedings of the 2003 Beam-Beam Workshop, Montauk, New York (2003).
16. Workshop on “RHIC II Physics and Perspectives for a New Comprehensive Detector”, Yale University, April 16 and 17, 2004 (http://star.physics.yale.edu/users/bump/April2004RHICworkshop%20folder/April2004RHICworkshop/)

3 Reports

3.1 Summary of the Workshop on the Physics of Seeded FELs

Kwang-Je Kim, ANL
mail to: kwangje@aps.anl.gov)

This workshop addressed the exciting physics and technology surrounding generation of longitudinally coherent XUV and x-ray pulses by free electron lasers (FEL) initiated by external coherent seed radiation. The primary FEL method proposed for generating such pulses was the "harmonic cascades" approach, where a transform-limited conventional laser seeds an initial FEL amplifier at UV wavelength. The FEL then produces harmonics that are amplified and successively frequency-multiplied in a series of stages eventually reaching the x-ray region of 0.1 - 10 nm. The workshop focused on methods for the generation of coherent output pulses with either very short time duration (<1 fs) or narrow relative line width (~1.e-6), and examined the many physics and technology issues to be addressed for combining the necessary short wavelength input laser and accelerator technology. The primary method of obtaining short wavelength laser input seed radiation is the use of high harmonic generation (HHG) in a noble gas.

A diverse group of 45 scientists and engineers from the fields of ultrashort lasers, accelerator physics, and FEL research representing academic and research institutions from around the world were invited to attend the 2 1/2 day workshop, held June 17 – 19, 2004 on the MIT campus. The agenda was structured to present several short talks on a subject, followed by discussion by the broader group. The presentations, as well as the agenda and attendees list, are available on the workshop website at http://mitbates.mit.edu/xfel/conference.htm.

Among the primary workshop goals were to:

i. identify factors that might degrade the performance of seeded FELs, such as timing jitter, variations in seed or electron beam parameters, and radiation noise growth in harmonic cascades

ii. define near-term proof-of-principle laser and FEL experiments that might be carried out at existing facilities

iii. address issues relevant to the timing and synchronization of multiple beams over the large distances and noisy electromagnetic environment of a major accelerator facility

iv. increase communication and collaboration between groups working in the short wavelength laser and FEL fields

The workshop discussions showed many interesting results, including generation of stable HHG XUV pulses with 5% energy fluctuation, longitudinal and transverse coherence measurements of HHG output, extraordinarily precise timing synchronization of less than 1 fs across multiple lasers, new theoretical results in the propagation and amplification of undesirable radiation noise in harmonic cascades, a semi-analytic design tool for optimizing harmonic cascades, the status and underlying physics approximations of several numerical simulation codes used to design and study expected cascade performance, and ongoing experimental results from the BNL DUV-FEL facility (itself a single stage FEL harmonic cascade), as well as plans for seeding experiments at several facilities both in Europe and the US.

3.2 Summary of the Workshop on XFEL Short Bunch Measurements and Timing

Patrick Krejcik, SLAC
mail to: pkr@SLAC.Stanford.EDU

The ICFA Future Light Sources Subpanel Miniworkshop on XFEL Short Bunch Measurement and Timing was held at the Stanford Linear Accelerator Center on July 26 - 30, 2004. It was convened jointly between SLAC, by John Galayda from the LCLS Division, and DESY by Joerg Rossbach from the TTF collaboration, and Argonne National Laboratory, by Kwang-Je Kim from the APS.

The ICFA Future Light Sources Subpanel has sponsored a number of workshops focusing on accelerator issues critical to the development of free electron lasers that will operate in the hard x-ray regime. The LCLS has jointly organized several of these with the European XFEL project centered at DESY in Hamburg Germany. This workshop focused on issues that will be critical to the optimal utilization of the short pulses (~ 100 fs) that these machines will deliver.

The organization and program committee consisted of Jerry Hastings (SSRL), Patrick Krejcik (LCLS), Holger Schlarb (DESY) and Juhao Wu (SLAC). Approximately 60 participants from all over the world took part.

Talks were solicited on three primary themes relating to the issues of measuring and synchronizing ultra-short bunches in linac-based FELs:

- Measurement techniques for determining the electron bunch length and arrival time.

- Measurement techniques, theory and simulation for diagnosing spontaneous undulator and XFEL radiation to determine its temporal profile.
- Issues of timing and synchronization of ultra-fast lasers to the electron bunch and RF.

Approximately one day was given to each of the themes listed above, with the first day dedicated to overview talks introducing each topic, plus talks on recent results from short bunch measurements from the various facilities. The invited talks were followed by extensive discussion sessions. The final day was given over to summarizing these discussions.

Highlights from the presentations included new ideas for distributed timing systems based on using lasers and optical fibers, as compared to conventional coaxial distribution systems based on quartz crystal oscillators as the master clock. There was also focus on electron beam bunch length diagnostics where electro-optic sampling at the SPPS facility at SLAC has recently demonstrated time resolution below 300 fs, with the clear possibility of extending this down to ~ 50 fs. Also discussed were ideas of using the x-ray photon beam to excite carriers in semiconductors and inserting this material as an active element in a laser interferometer. The discussion on all these issues was lively.

Further details of the workshop can be found at:

http://www-ssrl.slac.stanford.edu/lcls/xfel2004/

The next mini-workshop in this series will be held at DESY-Zeuthen (near Berlin) on April 18-22, 2005 and will be focused on commissioning issues of X-ray FELs. People interested in receiving an invitation should contact galayda@slac.stanford.edu or joerg.rossbach@desy.de

3.3 Report from the Working Group on Remote Experiments in Accelerator Physics

3.3.1 General Activities

Activities of the REAP working group during the past year include a mini-workshop at Trieste in November, 2003, work on webcasts of accelerator physics seminars, several R&D projects in remote operations and collaboration, and background activities in remote monitoring and control at most labs.

Several formal projects in remote control/operation of accelerators have gotten underway this year. The most comprehensive is the GANMVL (**M**ulti-purpose **V**irtual **L**aboratory) project initiated by a collaboration of EU laboratories with leadership by F. Willeke (DESY). This is a multifaceted project addressing critical aspects of remote operations and collaboration in a comprehensive plan. It has been this year approved for funding by the EU in the 6th Framework Program as part of the EuroTeV project. Another extensive project is Grid enabled Remote Instrumentation with Distributed Control and Computation to be carried out at the Elletra laboratory in Trieste. The CESR-Alfred University experiment in accelerator instrumentation in the US will

introduce university level students to accelerator physics through beam physics experiments carried out from their home institution. Further details on these and other projects are below.

There are multiple ongoing projects employing network communications around the labs in addition to these new initiatives. Many involve development and use of remote collaboration tools such as videoconferencing and file sharing. Nearly all laboratories support remote monitoring from the homes of staff members, and many support remote intervention to fix problems. Virtual Private Networks and SSL secure transmission are frequently used, as well as VNC for connection to local computers. For video conferencing VRVS is the most popular of the "non-commercial" systems.

3.3.2 Webcast Seminars

Work is continuing to establish a network of shared accelerator physics seminars. Several seminars were webcast from the Laboratory for Elementary-Particle Physics (LEPP) at Cornell. Information and archives may be accessed at http://www.lns.cornell.edu/public/COMP/AWSem/index.html. A suggestion (thanks to T. Satogata) has been made to provide a central location for links to all accelerator seminar schedules. These are being collected and are reachable on the REAP web site http://www.lns.cornell.edu/public/icfa/REAP/.

3.3.3 Workshop Report - CoToGAN 2003

The 3rd International Workshop on Communication Tools for a Global Accelerator Network, CoToGAN 2003, was held in Trieste, Italy, hosted by the Elettra laboratory, cosponsored by DESY and ICFA as a mini-workshop. 42 participants met in the Jolly Hotel in down town Trieste, 8 from the US and the balance from the EU and CERN. Topics covered included the proposed GAN/MVL project, reports on experience and plans in remote operations/diagnostics at various labs, distant collaboration issues such as desktop video conferencing, social and psychological aspects, and future directions of remote monitoring/control/operations.

Three working groups covered areas of 1) accelerator experiments with remote participation, 2) controls, networking, and accelerator hardware issues relevant for remote operations, and 3) technical, sociological, and operational aspects of telepresence.

The original workshop website is http://www.elettra.trieste.it/cotogan2003/ . Formal proceedings have not been published. A comprehensive collection of materials presented at the workshop is available online at http://ulisse.elettra.trieste.it/cotogan/.

3.3.4 Report on GANMVL Status

Ferdinand Willeke, DESY
mail to: ferdinand.willeke@desy.de

The linear collider will most likely be built within an international collaboration of several institutions. The other alternative, combining the necessary funding for building and operating the accelerator in a single laboratory appears to be less likely at this point. This means, that at least 50% of the facility will be provided by remote collaborators.

Extrapolating from HERA experience, it seems to be unlikely that the responsibility for the entire facility can be taken over by the site laboratory because of lack of expertise and human resources. It appears to be a more viable procedure that the contributing institutions will remain in charge of commissioning, operating, maintaining, trouble-shooting and performance optimizing of the systems they have designed and built. Since it might be very difficult in general to relocate the experts of the contributing laboratory to the site of the accelerator for an extended period of time, many of the listed activities on site might have to be done from remote locations.

For this mode of operation, there is only limited experience available in the accelerator community. While large detector systems have been built by international collaborations and part of detector operation has been performed by remote access, accelerator operations have only been performed and organized by the site laboratory of the accelerator.

It will be very important to explore the particular difficulties and challenges connected to remote operation of an accelerator (operation in the widest sense including the activities mentioned above) in order to make a reasonable choice on the way a large, international accelerator collaboration is constituted. This is the reason why we have to study remote operating and related topics at this point.

The GANMVL project tries to address these issues. GANMVL plans to provide a novel communication tool (Multi-purpose Virtual Laboratory) and apply it in accelerator environments. The communications tool will integrate video and audio capture and reproduction with secure and controlled access to accelerator controls and virtual instruments.

The tool should provide a remote user with the possibility to participate in many types of accelerator activities:

- ✓ Accelerator experiments and studies and tests performed from the accelerator control room
- ✓ Installation and assembly of accelerator components in a laboratory environment, in the accelerator tunnel or in service buildings
- ✓ Trouble shooting of accelerator components and many more.

GANMVL is configured in a server-client configuration. The server will be installed in a mechanical set up which is easily transportable. It has large video screens, camera and microphone systems attached to it. It will be easy to connect it to a local LAN and to various types of measurement equipment. The integrating software will automatically configure the system. The remote user will be provided with client programs which will run on his laptop, his office workstation or on a stationary videoconference system.

Among the special features that are envisioned for GANMVL, is the support of 3D video (which may be especially useful for capturing an assembly process or trouble shooting on accelerator components), multi-party videoconference based on advanced protocols, plug and play option for virtual instruments and convenient self-configuring operations software.

The GANMVL collaboration includes the DESY, GSI accelerator laboratories in Germany, INFN and the Elettra synchrotron light source laboratory in Italy and the universities of Udine, Italy and Manheim Germany.

The project has three phases: An exploratory and design phase, during which the input of the accelerator community will be included into the design of the MVL tool, a prototyping phase which will produce several prototypes of the MVL tool and finally an

application phase during which the MVL tools will be tested in several accelerator locations.

The project will extend over three years. As part of the EuroTev design study for a future linear collider, it has been approved for funding by the European Union in the 6th Framework Program. The project will be funded with approximately 1M. This will be matched by contributions of more than the same amount by the collaborating partner institutions. The project is expected to start up in January 2005.

3.3.5 Remote Operations Activities at Elettra

Roberto Pugliese
mail to: pugliese@elettra.trieste.it

We have completed the contract negotiation with European Community for a project GRIDCC (Grid enabled Remote Instrumentation with Distributed Control and Computation) aimed at extending grid middleware to support real-time an interactive applications. The middleware will be tried in test applications, one of which is the Remote Control of Elettra, the other the control of CMS detector at LHC (CERN). The project is a 3 year project (presented at CoToGAN2003) and among the participants there are Elettra, IBM, Imperial College, INFN.

The project will start on September 1st. The website is:

https://ulisse.elettra.trieste.it/gridcc.

In the context of this project we will setup at Elettra an AccessGRID node (the second in Italy) to test these technologies to evaluate the state of the art and possibly find the optimum solution for GRIDCC.

The Elettra Virtual Collaboratory by itself has developed significantly. We are now moving to webservices and many experimental stations have been equipped with EVC nodes. We have now the commitment to use EVC to allow remote operations of the accelerator and we have formed a task force including people from software, machine controls and operations (Emanuel Karantzoulis) to set up very quickly a prototype. I hope to have a first full prototype running by mid September. Emanuel Karantzoulis is olso defining details to test the prototype from Greece and Korea.

EVC derivatives will be also used in the context of the High Throughput Protein Crystallography EU project Bioxhit (http://www.embl-hamburg.de/BIOXHIT/) to implement a Virtual Collaboratory System where the experimental station can be relocated to the many different labs participating in the project.

3.3.6 CESR-Alfred Experiments in Accelerator Physics

This project was initiated by R. Holtzapple holtzapple@alfred.edu, a faculty member of Alfred University, to carry out accelerator physics research on the e+-e- storage ring at Cornell University, approximately 140 km distant. Support from the US National Science Foundation has been awarded to purchase and install streak camera and gated video camera instrumentation at CESR and implement a remote control facility at Alfred University. This project will involve both graduate and under-graduate students in physics. As of September 2004 work has been on implementation

of access to instrument control computers using VNC and setup of equipment. Full remote data acquisition and equipment/accelerator control is planned for spring, 2005.

4 Announcements of the Beam Dynamics Panel

4.1 ICFA Beam Dynamics Newsletter

4.1.1 Aim of the Newsletter

The ICFA Beam Dynamics Newsletter is intended as a channel for describing unsolved problems and highlighting important ongoing works, and not as a substitute for journal articles and conference proceedings that usually describe completed work. It is published by the ICFA Beam Dynamics Panel, one of whose missions is to encourage international collaboration in beam dynamics.

Normally it is published every April, August and December. The deadlines are 15 March, 15 July and 15 November, respectively.

4.1.2 Categories of Articles

The categories of articles in the newsletter are the following:

1. Announcements from the panel.
2. Reports of Beam Dynamics Activity of a group.
3. Reports on workshops, meetings and other events related to Beam Dynamics.
4. Announcements of future Beam Dynamics-related international workshops and meetings.
5. Those who want to use newsletter to announce their workshops are welcome to do so. Articles should typically fit within half a page and include descriptions of the subject, date, place, Web site and other contact information.
6. Review of Beam Dynamics Problems: this is a place to bring attention to unsolved problems and should not be used to report completed work. Clear and short highlights on the problem are encouraged.
7. Letters to the editor: a forum open to everyone. Anybody can express his/her opinion on the beam dynamics and related activities, by sending it to one of the editors. The editors reserve the right to reject contributions they judge to be inappropriate, although they have rarely had cause to do so.
8. Editorial.

The editors may request an article following a recommendation by panel members. However anyone who wishes to submit an article is strongly encouraged to contact any Beam Dynamics Panel member before starting to write.

4.1.3 How to Prepare a Manuscript

Before starting to write, authors should download *the latest* model article file, in Microsoft Word format, from the Beam Dynamics Panel home page (available soon)

http://www-bd.fnal.gov/icfabd/

It will be much easier to guarantee acceptance of the article if the latest model is used and the instructions included in it are respected. These model files and instructions are expected to evolve with time so please make sure always to use the latest versions.

The final Microsoft Word file should be sent to one of the editors, preferably the issue editor, by email.

The editors regret that LaTeX files can no longer be accepted: a majority of contributors now prefer Word and we simply do not have the resources to make the conversions that would be needed. Contributions received in LaTeX will now be returned to the authors for re-formatting.

In cases where an article is composed entirely of straightforward prose (no equations, figures, tables, special symbols, etc.) contributions received in the form of plain text files may be accepted at the discretion of the issue editor.

Each article should include the title, authors' names, affiliations and e-mail addresses.

4.1.4 Distribution

A complete archive of issues of this newsletter from 1995 to the latest issue is available at

http://icfa-usa.jlab.org/archive/newsletter.shtml

This is now intended as the primary method of distribution of the newsletter.

Readers are encouraged to sign-up for to electronic mailing list to ensure that they will hear immediately when a new issue is published.

The Panel's Web site provides access to the Newsletters, information about Future and Past Workshops, and other information useful to accelerator physicists. There are links to pages of information of local interest for each of the three ICFA areas.

Printed copies of the ICFA Beam Dynamics Newsletters are also distributed (generally some time after the Web edition appears) through the following distributors:

Weiren Chou	chou@fnal.gov	North and South Americas
Rainer Wanzenberg	rainer.wanzenberg@desy.de	Europe* and Africa
Susumu Kamada	Susumu.Kamada@kek.jp	Asia** and Pacific

* Including former Soviet Union.

** For Mainland China, Jiu-Qing Wang (wangjq@mail.ihep.ac.cn) takes care of the distribution with Ms. Su Ping, Secretariat of PASC, P.O. Box 918, Beijing 100039, China.

To keep costs down (remember that the Panel has no budget of its own) readers are encouraged to use the Web as much as possible. In particular, if you receive a paper copy that you no longer require, please inform the appropriate distributor.

4.1.5 Regular Correspondents

The Beam Dynamics Newsletter particularly encourages contributions from smaller institutions and countries where the accelerator physics community is small. Since it is impossible for the editors and panel members to survey all beam dynamics activity world-wide, we have some *Regular Correspondents*. They are expected to find interesting activities and appropriate persons to report them and/or report them by themselves. We hope that we will have a "compact and complete" list covering all over the world eventually. The present *Regular Correspondents* are as follows

Liu Lin	liu@ns.lnls.br	LNLS Brazil
S. Krishnagopal	skrishna@cat.ernet.in	CAT India
Ian C. Hsu	ichsu@ins.nthu.edu.tw	SRRC Taiwan

We are calling for more volunteers as *Regular Correspondents*.

4.2 ICFA Beam Dynamics Panel Members

Caterina Biscari	caterina.biscari@lnf.infn.it	LNF-INFN, Via E. Fermi 40, C.P. 13, Frascati, Italy
Swapan Chattopadhyay	swapan@jlab.org	Jefferson Lab, 12000 Jefferson Avenue, Newport News, VA 23606, U.S.A.
Pisin Chen	chen@slac.stanford.edu	SLAC, P.O. Box 4349, MS 26, Stanford, CA 94309, U.S.A.
Weiren Chou (Chair)	chou@fnal.gov	Fermilab, MS 220, P.O. Box 500, Batavia, IL 60510, U.S.A.
Yoshihiro Funakoshi	yoshihiro.funakoshi@kek.jp	KEK, 1-1 Oho, Tsukuba-shi, Ibaraki-ken, 305-0801, Japan
Miguel Furman	mafurman@lbl.gov	Center for Beam Physics, Lawrence Berkeley National Laboratory, Building 71, R0259, 1 Cyclotron Road, Berkeley, CA 94720-8211, U.S.A.
Jie Gao	gao@lal.in2p3.fr	Laboratoire de L'Accélérateur Linéaire, B.P. 34, 91898 Orsay cedex, France
Ingo Hofmann	i.hofmann@gsi.de	High Current Beam Physics, GSI Darmstadt, Planckstr. 1, 64291 Darmstadt, Germany
Sergei Ivanov	ivanov_s@mx.ihep.su	Institute for High Energy Physics, Protvino, Moscow Region, 142281 Russia
Kwang-Je Kim	kwangje@aps.anl.gov	Argonne National Laboratory, Advanced Photon Source, 9700 S. Cass Avenue, Bldg 401/C4265, Argonne, IL 60439, U.S.A.
In Soo Ko	isok@postech.ac.kr	Pohang Accelerator Laboratory, San 31, Hyoja-Dong, Pohang 790-784, South Korea
Alessandra Lombardi	Alessandra.Lombardi@cern.ch	CERN, CH-1211, Geneva 23, Switzerland
Yoshiharu Mori	Yoshiharu.mori@kek.jp	KEK, 1-1 Oho, Tsukuba-shi, Ibaraki-ken, 305-0801, Japan
David Rice	dhr1@cornell.edu	Cornell University, 271 Wilson Laboratory, Ithaca, NY 14853-8001, U.S.A.
Yuri Shatunov	Yu.M.Shatunov@inp.nsk.su	Acad. Lavrentiev, prospect 11, 630090 Novosibirsk, Russia
Junji Urakawa	junji.urakawa@kek.jp	KEK, 1-1 Oho, Tsukuba-shi, Ibaraki-ken, 305-0801, Japan
Jie Wei	wei1@bnl.gov	BNL, Bldg. 911, Upton, NY 11973- 5000, U.S.A.
Jiu-Qing Wang	wangjq@mail.ihep.ac.cn	Institute for High Energy Physics, P.O. Box 918, 9-1, Beijing 100039, China
Rainer Wanzenberg	Rainer.wanzenberg@desy.de	DESY, Notkestrasse 85, 22603 Hamburg, Germany

The views expressed in this newsletter do not necessarily coincide with those of the editors. The individual authors are responsible for their text.